

Surface UV radiation over Australia, 1979–1992: Effects of ozone and cloud cover changes on variations of UV radiation

Petra M. Udelhofen¹

Cooperative Research Centre for Southern Hemisphere Meteorology, Monash University,
Melbourne, Australia

Peter Gies and Colin Roy

Australian Radiation Protection and Nuclear Safety Agency, Melbourne, Australia

William J. Randel

National Center of Atmospheric Research, Boulder, Colorado

Abstract. Time series of daily erythemal ultraviolet radiation (UVR) exposure, ozone, and cloud cover were analyzed over the Australian continent using data sets from the NASA Total Ozone Mapping Spectrometer (TOMS) from 1979–1992. The TOMS UVR exposures showed good agreement with data from surface observations. Using a relationship derived from comparisons of the TOMS partial cloud reflectivities with surface cloud cover observations, the TOMS reflectivities were converted into estimates of cloud cover for several Australian regions. It was shown that the deseasonalized time series of UVR exposures can be statistically described as a linear function of ozone and cloud cover anomalies. Results of a trend analysis indicated statistically significant increases in UVR exposures of 10% decade⁻¹ in the summer months in the tropics. These were associated with a simultaneous depletion of ozone and a decrease in cloud cover. Midlatitudinal regions showed no significant trends of UVR. It was found that variations of ozone and UVR over Australia were significantly influenced by the quasi-biennial oscillation (QBO). An increase in zonal wind strength of 20 m s⁻¹ was correlative with reductions of ozone of 1.7% and enhancements of UVR exposures of 2.2%. An increase in solar radio flux of 100×10⁻²² W m⁻² (Hz)⁻¹ was associated with significant reductions of UVR of 5–10% in the tropical and subtropical regions in summer. The results suggested that enhancements in summer UVR exposures of about 10–20% above the climatological average might be expected in years in which the QBO is in its westerly phase and the solar cycle is at its minimum.

1. Introduction

Ultraviolet radiation (UVR) in the wavelength range between 280 and 315 nm (UV-B) has a profound impact on erythema, skin cancer, and plant damage. Over the tropical parts of Australia, incidences of skin cancer rank amongst the highest in the world and are surpassed only by New Zealand and parts of the populations in Hawaii [Giles and Thursfield, 1996; Kricker and Armstrong, 1996]. Although there are signs that the rate of

increase has slowed down [Giles and Thursfield, 1996], there is still considerable concern that the increases in incidences of skin cancer are linked to changes in surface UV-B radiation as a result of ozone depletion. Recently, attempts have been made to model the increase in non-melanoma skin cancer as a function of changes in UV-B radiation due to ozone depletion [Williams and Green, 1996]. These epidemiological studies require the determination of UV-B doses (daily integrated UVR exposures) within demographic regions as defined in Figure 1 so they can be compared to cancer statistics.

Ozone depletion is one of several factors that affect the variability of UV surface radiation. The maximum instantaneous clear-sky UV irradiance is observed at local solar noon, when the sun is highest in the sky. The seasonal cycle of daily integrated UVR exposures has amplitudes of the same order as the annual mean, which can be attributed mostly to seasonal changes in

¹Now at Institute for Terrestrial and Planetary Atmospheres, State University of New York, Stony Brook, New York.

Copyright 1999 by the American Geophysical Union.

Paper number 1999JD900306.
0148-0227/99/1999JD900306\$09.00

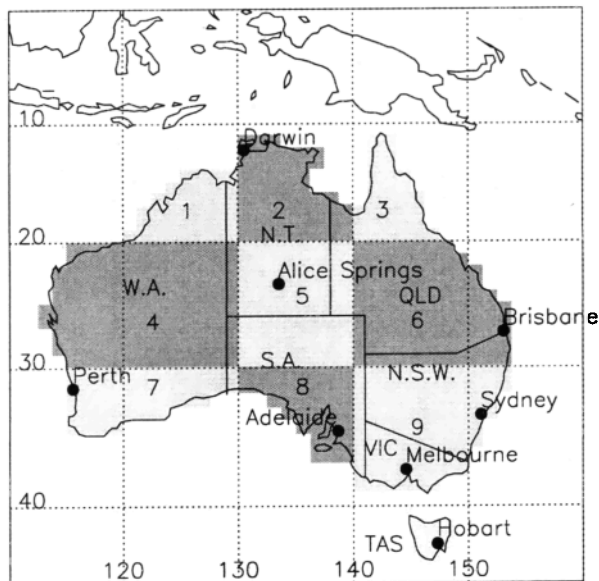


Figure 1. Map of Australia indicating the Australian States, New South Wales (N.S.W.), Northern Territory (N.T.), Queensland (QLD), South Australia (S.A.), Tasmania (TAS), Victoria (VIC), and Western Australia (W.A.), with solid lines indicating state boundaries. Shaded areas denote the regions used for further analysis. These are identified 1-9 with Tasmania being the tenth area and identified as "0." Also indicated are the location of stations for which surface UVR and cloud measurements were obtained.

the maximum solar elevation and the length of the day. For a given solar elevation the absorption of ozone is the dominant factor determining clear-sky UVR values. The effect of relative ozone changes on the surface UV radiation can be expressed in terms of a radiation amplification factor [McKenzie *et al.*, 1991].

Clouds and aerosols scatter the UV radiation. For a further description of the budget of biologically active UVR, refer to Frederick and Lubin [1988]. The presence of aerosols can cause substantial UVR reductions on clear days. These effects are pronounced locally in strongly polluted areas, regionally in areas affected by smoke plumes from biomass burning or desert dust, and globally after volcanic eruptions. Surface UVR enhancements may be observed as a result of trapping of photons between an aerosol layer and a highly reflective surface [Michelangeli *et al.*, 1992; Shettle and Weinman, 1970]. Clouds are the most prominent scatterers of UV radiation; thus knowledge of the spatial and temporal variabilities of cloud cover and cloud type are very important for an understanding of the variabilities of UVR. The effect of cloud cover on the surface UV radiation is very complex. Measurements have shown that homogeneous cloud layers lead to a reduction of surface UVR [Schafer *et al.*, 1996; Frederick and Snell, 1990; Estupiñán *et al.*, 1996; Seckmeyer *et al.*, 1996]. A partially cloudy sky with an unobstructed direct solar

beam, however, can lead to an enhancement of surface UVR due to reflection of solar radiation at the sides of clouds [Estupiñán *et al.*, 1996; Schafer *et al.*, 1996; Mims and Frederick, 1994].

The effects of UV radiation on biological systems have been reviewed by Madronich [1993]. Furthermore, Madronich [1992] used TOMS ozone data to estimate zonally averaged trends of biologically effective UV radiation under clear skies for different biological action spectra. In the past, two studies specifically tried to estimate UVR trends in Australia. Roy and Gies [1989] applied a semi-empirical model based on Green *et al.* [1974b] and Green *et al.* [1974a] to estimate the sensitivity in local solar-noon UV-B radiation to percentage changes in total ozone for eight cities in Australia using climatological ozone values by Dütsch [1971]. Subsequently, Bodeker [1993] derived a statistical model using TOMS data to predict monthly mean ozone values for Australian and New Zealand cities up to the year 2000. The model includes a trend, an annual variation, a quasi-biennial oscillation (QBO), a solar cycle component, and a semiannual signal. To predict clear-sky local solar noon erythemal UV radiation values, a model based on Iqbal [1983] and McKenzie [1991] was used. Both studies discussed clear-sky UV radiation changes and did not include cloud cover.

Lubin and Jensen [1995] investigated whether ozone trends would lead to significant trends in biologically effective UV radiation at local solar noon when taking into account the effect of cloud variabilities on UVR. They predicted that because of the variability being sufficiently small in temperate regions of Australia, "by the end of this century, trends in summer average local-noon UVR dose rates relevant to mammalian skin cancer or plant damage should be significant with respect to cloud variability." (p. 710).

It will be investigated whether this thesis holds for the erythemal UVR doses by analyzing TOMS-derived erythemal UVR exposure data over Australia. Herman *et al.* [1996] calculated and discussed zonally averaged trends of daily integrated UVR exposure. The data used here are TOMS erythemal UVR exposures, a revised version of the original TOMS UV data set [Herman and Celarier, 1996]. The erythemal weighting was performed with the action spectrum of McKinlay and Diffey [1987]. It will be shown that the TOMS UVR exposure anomalies can be approximated as a linear function ozone and cloud amount anomalies over the Australian region. To derive this relationship, the TOMS ozone data (version 7) are used, and cloud amounts are inferred from the TOMS reflectivity data [McPeters and Beach, 1996a, b].

As a first step, the TOMS daily integrated UVR exposure data are evaluated by comparing them to surface UVR measurements. A relationship between the TOMS reflectivity and cloud amount is derived at eight stations in Australia (see Figure 1) from comparisons of colocated TOMS reflectivity measurements and sur-

face cloud cover observations. The TOMS partial cloud reflectivities are then converted into estimates of total cloud cover. Next, the climatology and seasonal cycles of UVR, ozone, and cloud cover are derived, and the deseasonalized time series are calculated. These are used as input for the trend analysis. Monthly and annual trends, as well as components associated with the quasi-biennial oscillation (QBO), the solar cycle, and the El Niño–Southern Oscillation (ENSO) are inferred separately for the UVR exposures, ozone, and cloud amounts. The analyses are carried out for several Australian regions and the entire continent.

2. Evaluation of TOMS Data With Surface Measurements

2.1. Measurements of UVR Exposures in Australia

Although several UVR networks have existed in Australia in the past, a consistent long-term data record of UV-B measurements does not exist at present. Between 1963 and 1970, Robertson [1972] operated a small network of broadband instruments, the predecessors of the Robertson-Berger meters. To test an alternative broadband detector for suitability of monitoring long-term changes in UVR, a different broadband UV-B network was established and operated between 1975 and 1981 at five Australian stations and one station in Papua New Guinea [Barton, 1983; Paltridge and Barton, 1978]. The UVR detectors provided sufficient data to allow the derivation of a geographic and seasonal climatology of UV-B [Paltridge and Barton, 1978] but were considered unsuitable to monitor long-term changes. Recently, Weatherhead *et al.* [1997] came to a similar conclusion for the Robertson-Berger network in the United States.

After the discovery of the ozone hole over Antarctica [Farman *et al.*, 1985] the proximity between the Australian and Antarctic continents led to concerns that the ozone hole would affect the ozone distribution and hence the UV radiation in Australia. Moreover, it was speculated whether the concurrent increase in skin cancer rates in Australia could be attributed to the effects of the ozone hole [National Health and Medical Research Council, 1989]. As UVR measurements were not available at the time, the present broadband UVR network operated by the Australian Radiation Laboratory (ARL) [Roy *et al.*, 1995] was initiated to address this question. Data from the ARL network overlap with the TOMS data record and will be used for evaluation.

2.1.1. Surface UVR measurements from the ARL network. The ARL network includes a number of different UVR detectors. Measurements with an International Light (IL) UV actinic detector (IL ACTS) were available from the middle of the 1980s. These instruments measure the biological effective irradiance. Their naming is somewhat confusing as they

do not measure the actinic fluxes. The improper use of the term “actinic flux” has been discussed in detail by Madronich [1987]. Nevertheless, part of the literature employs the term “actinic” to define the spectral region between 200 and 315 nm [*American Conference of Governmental Industrial Hygienists (ACGIH)*, 1980; *International Light*, 1991 (available at <http://www.Intl-Light.com/products/uvhazard.html>); *Ryer*, 1997 (available at <http://www.Intl-Light.com/handbook/>)]. In spite of the difference in semantics it should be kept in mind that the IL instruments measure the UV irradiance with a spectral response that is similar to the erythemal response (action spectrum) defined by the ACGIH, [1980]. This response has been adopted by the International Radiation Protection Association (IRPA) as a standard action spectrum [Duchêne *et al.*, 1991]. Furthermore, their definition is very similar to the erythemal response of McKinlay and Diffey [1987] adopted by the International Commission on Illumination [*Commission Internationale de l'Éclairage (CIE)*, 1991]. The action spectrum of McKinlay and Diffey [1987] has been used to derive the TOMS erythemal exposure data. Although these different weightings result in differences of absolute irradiance, for solar zenith angles less than 60° the differences can be adjusted by employing a constant factor. Results from radiative transfer calculations showed that the CIE-weighted irradiance is approximately 0.78 ± 0.01 times the IL irradiance. The two-stream approximation of the radiative transfer model UVspec (A. Kylling, UVspec: A program package for calculation of diffuse and direct visible intensities and fluxes, 1995; available by anonymous ftp to [kaja.gi.alaska.edu, cd pub/arve](http://kaja.gi.alaska.edu/cd/pub/arve)) (Hereinafter referred to as Kylling, 1995) [Kylling *et al.*, 1995] has been used to perform these calculations. The model calculations were performed for clear sky conditions using the total ozone from TOMS and setting the visibility to 15 km to account for aerosols.

To convert the photon counts measured by the surface instruments into absolute irradiance, regular calibrations of these instruments would be desirable but are not available for all instruments on a sufficiently routine basis. Therefore model calculations were used to calibrate the data vicariously. Two models were employed for verification of these calibrations, that is, UVspec [Kylling, 1995] and a model by Björn [1989]. The counts were converted into CIE-weighted irradiances using calibration factors derived from model calculations at local solar noon. It was found that these calibration factors did not account for the decrease in instrument sensitivity with increasing solar zenith angle [Roy *et al.*, 1996] and resulted in an underestimation of the daily doses. To account for this bias, correction factors for daily exposures were determined for each instrument by comparing daily integrated measurements on clear sky days to modeled daily total exposures using UVspec. The correction factors vary between 1.05 and 1.46, depend-

Table 1. Cosine Correction Factors for the Surface International Light Measurements Derived From Comparisons of the Daily Integrated Surface Measurements With Model Calculations on Clear-Sky Days

Station (Latitude, Longitude)	Number of Clear-Sky Measurements	Cosine Correction Factors
Darwin (-12.5, 130.8)	122	1.18 ± 0.07
Alice Springs (-23.4, 133.5)	760	1.25 ± 0.14
Brisbane (-27.5, 153.1)	225	1.29 ± 0.18
Perth(-31.9, 115.9)	175	1.19 ± 0.08
Sydney (-33.9, 151.2)	131	1.05 ± 0.13
Adelaide (-34.7, 138.6)	44	1.22 ± 0.10
Melbourne(-38.0, 145.1)	170	1.29 ± 0.12
Hobart (-42.8, 147.5)	32	1.46 ± 0.13

ing on instrument and location. Details are listed in Table 1. The daily integrated irradiances were multiplied with these factors to adjust for the nonideal cosine response of the instruments.

In summary, to obtain the daily doses (erythemal exposures) from surface observations, the measured counts were first converted into erythemally CIE-weighted irradiances using calibration factors derived from model calculations at solar noon and then adjusted with cosine correction factors as listed in Table 1. These values will be compared to the TOMS erythemal exposures. Their derivation is described in the next section.

2.1.2. TOMS erythemal UVR exposure algorithm. The TOMS UVR exposure data have been obtained from NASA Goddard Space Flight Center (GSFC). In order to evaluate this data with measurements from the surface network, a brief discussion of the TOMS algorithm will be given based on *Herman et al.* [1996] and *Herman and Celarier* [1996]. As discussed by *Herman et al.* [1996], the TOMS erythemal UVR exposures have been calculated with a radiative transfer model. Input variables were the TOMS ozone data, surface albedos estimated from the Lambertian Equivalent Reflectivities (LER) [*Herman and Celarier*, 1997], and an estimate of cloudiness as follows. The TOMS algorithm uses reflectivity measurements at 380 nm to identify cloudy scenes. Then a cloud optical depth is deduced from the 380 nm reflectivity assuming a uniform cloud layer “homogeneously distributed in a slab between 500 and 700 mb” for each pixel [*Herman and Celarier*, 1996, readme file]. The UV spectral irradiance of a cloudy scene is calculated by applying a cloud correction factor (a function of the cloud optical depth, surface reflectivity, terrain height, and solar zenith angle) to the clear-sky spectral irradiance [*Herman et al.*, 1996]. Erythemally weighted irradiances have been derived using the action spectrum of *McKinlay and Diffey* [1987]. The daily integration has been carried out assuming no diurnal variation in cloudiness. TOMS UVR overpass data are now evaluated with surface measurements from eight stations.

2.1.3. Surface UVR intercomparison. Figure 2 shows the scatter diagrams of cosine-corrected surface measurements with colocated TOMS erythemal exposure data. TOMS UVR overpass data have been provided by NASA GSFC for intercomparison purposes. Table 2 summarizes the statistics of the intercomparison. The correlations between these measurements are larger than 0.76 and above 0.9 for most stations. Aerosols are not considered in the TOMS UV algorithm, which could explain the slight overestimation of TOMS erythemal UVR compared to the surface measurements. Furthermore, the TOMS UV algorithm does not take into account a diurnal variability in cloud cover. Using the argument of ergodicity (*E. Celarier*, personal communication, 1998), it was assumed that the spatial average across a TOMS pixel would approximate the temporal average at a single point. This assumption might not be accurate at tropical stations with a strong diurnal cycle of convection and might explain the

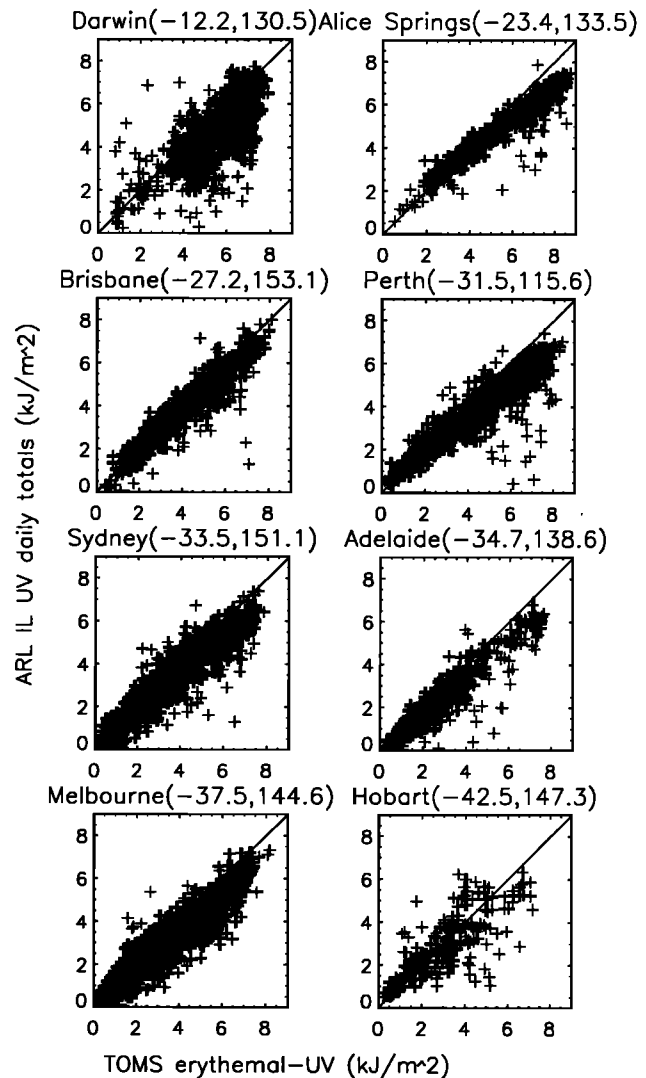


Figure 2. Comparison of Total Ozone Mapping Spectrometer (TOMS) erythemal daily total UVR exposures with surface measurements from the network of the Australian Radiation Laboratory (ARL).

Table 2. Intercomparison Between TOMS Erythemal UVR Exposures and Daily Integrated and Cosine-Corrected Surface Measurements for Eight Stations in Australia

Station	Data Points	TOMS - IL			r
		Average, J m^{-2}	Bias, $\text{J m}^{-2}(\%)$	S.D., $\text{J m}^{-2}(\%)$	
Darwin	1077	5148	690 (13)	926 (18)	0.76
Alice Springs	772	4835	482 (10)	656 (14)	0.97
Brisbane	599	3637	237 (7)	640 (18)	0.94
Perth	1152	3586	429 (12)	784 (22)	0.95
Sydney	1079	2967	248 (8)	671 (23)	0.94
Adelaide	401	2679	476 (18)	715 (27)	0.93
Melbourne	1596	2644	253 (10)	608 (23)	0.96
Hobart	214	2832	161 (6)	1076 (38)	0.79

TOMS, Total Ozone Mapping Spectrometer; UVR, ultraviolet radiation; IL, International Light; S.D., standard deviation.

The number of data points used in each intercomparison are listed in column 2. Column 3 tabulates the average UVR exposures of the colocated measurements. Columns 4 and 5 list the bias and standard deviation of the differences between TOMS and surface measurements in absolute (J m^{-2}) and relative (%) units. The last column indicates the correlation coefficient r between the two data sets.

larger discrepancy at Darwin. The biases between the TOMS and surface measurements range between 6 and 13%, and the standard deviations range between 10 and 38%, with Hobart the site with the largest standard deviation. Overall, the TOMS data compare well with the surface measurements.

2.2. TOMS Ozone Data

The TOMS version 7 ozone data have been evaluated extensively with Dobson stations [McPeters and Labow, 1996]. A closer look at the Australian Dobson stations reproduced the results as has been previously discussed by Atkinson and Easson [1989] and McPeters and Labow [1996]. Hence the TOMS version 7 ozone data will be used without further evaluation.

2.3. Estimation of Cloud Coverage From TOMS Reflectivity Data

It will be shown that TOMS partial cloud reflectivities can be used to derive an estimate of cloud amount over the Australian continent.

2.3.1. TOMS partial cloud reflectivities. The TOMS partial cloud reflectivities are derived from measurements of the backscattered radiance at 380 nm. The derivation is described in detail in the TOMS user's guide [McPeters et al., 1996], but a brief summary will be given here as background. The algorithm assumes that the measured radiances are reflected from two levels in the atmosphere, that is, the ground and the cloud top. For a given TOMS measurement at 380 nm (I_{measured}), the first step is to calculate radiances at 380 nm for reflection off the ground I_{ground} and reflection from the cloud I_{cloud} .

The latter implies an assumption of the cloud height, which is inferred from the climatology of the International Cloud Climatology Project (ISCCP) [Rossow and Schiffer, 1991]. A cloud reflectivity R_c of 0.8 is assumed. Given the ground terrain pressure, the surface radiance is estimated from radiative transfer calculations assuming a ground reflectivity R_g of 0.08 for snow- and ice-free conditions and 0.5 for snow/ice. If $I_{\text{ground}} \leq I_{\text{measured}} \leq I_{\text{cloud}}$ under snow- and ice free conditions an effective cloud fraction f is determined using $f = (I_{\text{measured}} - I_{\text{ground}})/(I_{\text{cloud}} - I_{\text{ground}})$. If snow/ice is assumed to be present, then the value of f is divided by 2. The TOMS partial cloud reflectivity R is derived from the cloud fraction

$$R = R_g(1 - f) + R_c f, \quad (1)$$

where R_g is the ground reflectivity conditions and R_c is the cloud reflectivity. If $I_{\text{measured}} < I_{\text{ground}}$, the backscattered radiation is thought to be entirely from the surface and is determined by solving the boundary condition of the radiative transfer equation [Dave, 1964]. Equation (1) thus implies a linear relationship between reflectivities and cloud amount in the absence of snow/ice.

It is investigated whether such a linear relationship can be observed over the Australian continent. It is possible, because Australia is virtually snow-free over the course of a year, with the exception of a few areas in the mountains smaller than the grid resolution of the reflectivity data. With the assumption that changes in surface reflectivities under snow-free conditions are small, the relationship between reflectivities and cloud amount should be linear if the clouds are optically thick. A lin-

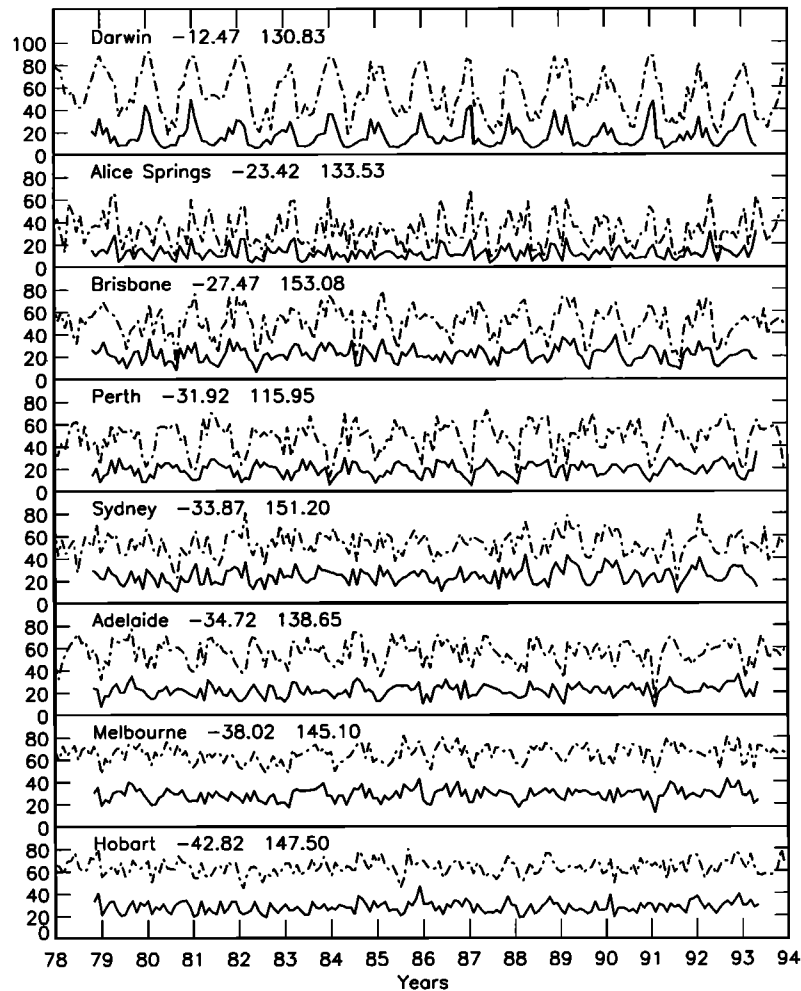


Figure 3. Time series of monthly mean total cloud cover from surface observations (dashed lines) and TOMS partial cloud reflectivities (solid lines) for eight stations in Australia.

ear relationship between the effective cloud fraction f and the reflectivity R follows from rearranging (1) and substituting $R_g = 0.08$ and $R_c = 0.80$. The effective cloud fraction is related to the partial cloud reflectivity by

$$f = -\frac{R_g}{R_c - R_g} + \frac{1}{R_c - R_g} R = f_0 + 1.4R, \quad (2)$$

with $f_0 = -11.1\%$.

2.3.2. Comparisons to surface cloud cover observations. The relationship between reflectivity and clouds is examined further by comparing TOMS partial cloud reflectivities with surface cloud observations. The surface cloud observations were obtained from the National Climate Centre of the Bureau of Meteorology for the eight stations discussed earlier (e.g., Figure 1). The data set consists of observations of total cloud cover, cloud types, and base heights at three-hourly intervals. From this data set the total cloud amounts at local noon were averaged to provide monthly mean values. Monthly averages of partial cloud reflectivities

at these stations were derived from TOMS overpass data. Figure 3 shows the monthly mean time series of surface observations and colocated TOMS reflectivity data. It is evident that the cloud observations and the reflectivity are correlated. To investigate this correlation, the data are presented as scatter diagrams in Figure 4. It becomes apparent that the reflectivities and cloud amounts in the extratropical stations (Figures 4b-4h) can be described as linearly correlated, whereas at the tropical station Darwin (Figure 4a) the relationship seems nonlinear. As Figure 4i indicates, a linear regression can be derived using all data of the extratropical stations. The resulting fit is drawn as a solid line in Figures 4b-4i. The regression equation relating surface cloud cover C to reflectivity R is given as $C = 11.1 + 1.9R$. Details of the statistics are listed in Table 3. The observed rate of change of cloud cover C as a function of reflectivity is slightly larger than in (2), and the difference between C_0 and f_0 is 22%.

A further analysis of the surface cloud cover data set reveals that these differences might be associated with multilayered cloud bands which are observed frequently

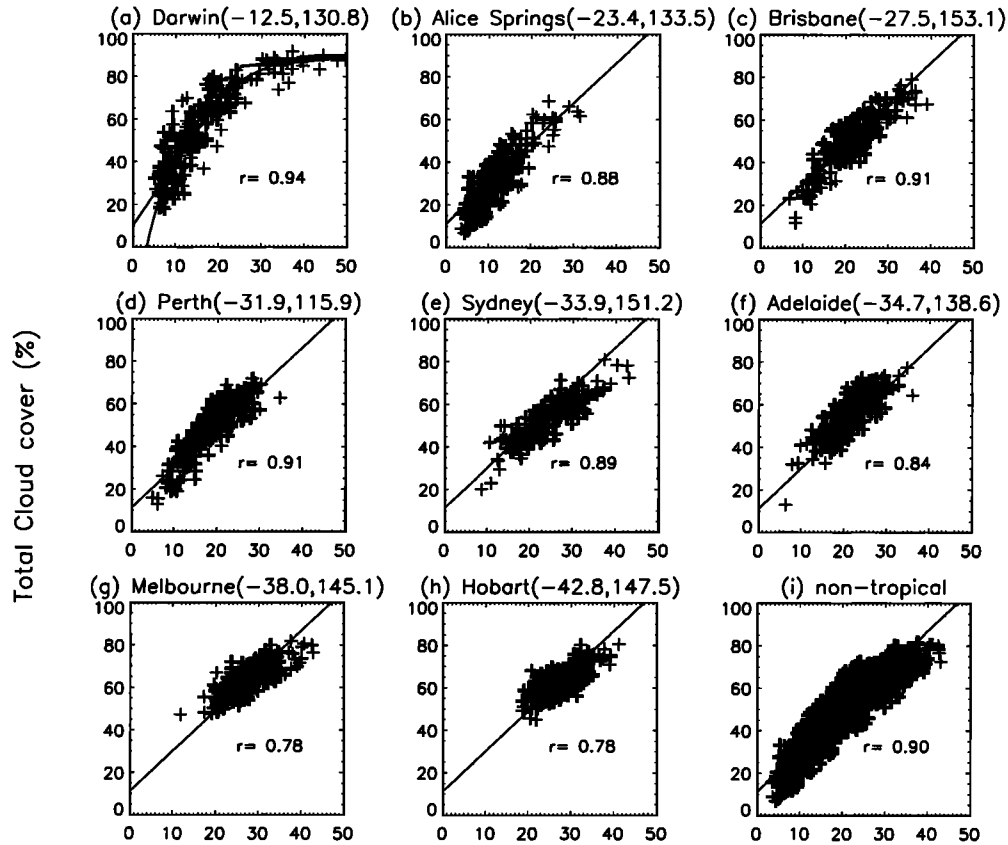


Figure 4. Monthly mean total cloud cover from surface observations compared with TOMS partial cloud reflectivities. Darwin, the only station in the tropics, shows a nonlinear relationship between surface observation and TOMS partial cloud reflectivities. All other stations can be described as linear. A relationship between surface cloud cover and reflectivities has been derived to convert the reflectivity into cloud cover. Results of a regression analysis are listed in Table 3.

at most stations, which (2) does not take into account. Each station is associated with a distinct range of reflectivities, which might be related to the prevalence of different cloud types. For example, Alice Springs is a station in the center of Australia and has a dry arid subtropical climate. Altocumulus and cirrus are the most frequent cloud types. On the east coast of Aus-

tralia, mountains of the Great Dividing Range form a natural boundary between the arid climate of central Australia and the humid climate on the east coast. Brisbane and Sydney are subtropical stations on the east coast. Perth, on the coastal region of Western Australia, is affected by tropical cyclones. Adelaide is located at the southeastern edge of the desert. At

Table 3. Average Reflectivity \bar{R} , Cloud Cover \bar{C} , and the Estimated Regression Coefficients to Determine Cloud Cover C From TOMS Reflectivity Measurements R

Station	\bar{R}	\bar{C}	C_0	a_1	a_2	Correlation Coefficient
Darwin						
$R < 25\%$	13.2	49.6	9.9	3.0 ± 0.4	–	0.86
$R > 25\%$	35.0	83.6	79.7	0.2 ± 0.4	–	0.87
	16.5	54.9	-77.0	-3.6 ± 1.0	48.7 ± 9.1	0.94
Extratropical	22.1	52.5	11.1	1.9 ± 0.3	–	0.90
All data	21.5	52.9	14.6	1.8 ± 0.2	–	0.87

For most stations a linear fit is sufficient to describe the relationship between the variables. At Darwin the relationship is more complex. The linear regression coefficients for two regimes, $R < 25\%$ and $R > 25\%$, are derived separately. A nonlinear regression equation $C = C_0 + a_1R + a_2\sqrt{R}$ can be used to describe the relationship over the entire range of R .

these four stations, low clouds (cumulus and stratocumulus) are the most frequently observed cloud types with midlevel type clouds (altostratus and altocumulus) and high-level clouds (cirrus) present. Although several layers are often present at the same time, they tend to cover different portions of the sky, and the overlap is small. Melbourne and Hobart are in a temperate climate where passages of cold fronts are commonly observed and multilayered cloud bands are recurrent. These results are generally consistent with the analysis of *Warren et al.* [1986]. Semitransparent midlevel and high-level clouds might be the cause of the underestimation of cloud cover from satellite and explain the differences of 22% between the two constants C_o and f_o (e.g., Table 3 and (2)).

At the tropical station Darwin (Figure 4a) the relationship between reflectivity and observed cloud cover is clearly nonlinear. It is found that these nonlinearities are associated with a seasonal change in cloud cover. The tropical monsoon leads to a pronounced seasonal cycle in the cloud amount at Darwin (see Figure 3), dominated by convective cloud types. To investigate the nonlinearities further, the data points were divided into two regimes, $R < 25\%$ and $R > 25\%$. Separate linear fits for the reflectivities $R < 25\%$ and $R > 25\%$ were derived, and the results are listed in Table 3. Reflectivities $> 25\%$ are observed during the summer season in January and February (see Figure 3). During that time period the midlevel and high-level cloud amounts increase by about 20%, that is, from 10 to 35% for midlevel clouds and from 40 to 65% for high-level clouds. The increase in low-level cloud amount is 15%, that is, from 50 to 65%. Low and high clouds are present in two layers covering the sky to 50%, on average. Midlevel clouds (altocumulus) are present with an amount of 17.2%, on average. It was found that a quadratic fit can approximate the reflectivity–cloud cover relationship. The results are listed in Table 3.

In summary, at extratropical stations a change in reflectivity of 1% results in a change in cloud amount of 1.9%. At Darwin a 3% change in cloud cover is associated with a 1% change in reflectivity outside the monsoon season. In the monsoon season a 1% increase in reflectivity results in a moderate increase in cloud amount of about 0.2%. As clouds cover nearly 100% of the sky, the change in reflectivity is most likely associated with the increase of highly reflective cloud types.

The regression coefficients (Table 3) are applied to estimate the cloud amount in subregions of the Australian continent. In tropical regions, the quadratic fit is used to convert the TOMS reflectivities into cloud amounts. Cloud amounts in extratropical regions are calculated from the linear regression given in Table 3.

2.4. Gridded TOMS Data Sets

The climatological and trend analyses discussed below are based on level 3 gridded TOMS data. The gridded data sets (UVR exposures, ozone, and partial

cloud reflectivities) have a resolution of $1.0 \times 1.25^\circ$ and are available for every day between November 1978 and May 1993. Whenever the terms UVR, ozone, and cloud cover are used hereafter, the TOMS erythemal UV exposures, the TOMS version 7 ozone data set, and the cloud amounts derived from TOMS partial cloud reflectivity data are implied.

3. TOMS UVR Climatology for Australia

As discussed earlier, the TOMS erythemal UVR exposures have been derived by weighting spectral irradiances with the action spectrum of *McKinlay and Diefey* [1987] and integrating the result over the length of day. From the gridded data set a climatology has been obtained for each month as well as annually, using all data from 1979 until the end of 1992. Australian contour maps are shown in Plate 1 for January, April, July, October, and the annual average. It is evident that during winter (i.e., July) daily UVR exposures are zonally symmetric over the continent and range from $< 0.5 \text{ kJ m}^{-2}$ in Tasmania to 4 kJ m^{-2} in the tropics. The months of April and October and the annual average show a slight asymmetry toward the eastern edge of the continent, which is most likely associated with the Great Dividing Range, the boundary between the humid climate on the east coast and arid climate at the Australian interior. The humid climate east of the Great Dividing Range leads to a reduction of the UVR exposures compared to the values west of the Dividing Range. In the summer, largest daily integrated UVR exposure data are found in the subtropical desert with extreme values above 7.8 kJ m^{-2} .

For further analysis the Australian continent is divided into nine regions plus Tasmania as a separate region. The zonal and longitudinal dependence of the UVR, ozone, and cloud variability will be investigated in detail for these regions.

3.1. Geographical Average

The nine regions over the Australian continent have been selected by taking into account climatic and geographical regimes (see Figure 1). Several studies using rainfall analysis have indicated that the climatic zones in Australia can be classified as tropical, subtropical, and temperate [*Bureau of Meteorology*, 1995; *Simmonds and Hope*, 1997]. These climatic classifications correspond approximately to the latitudinal bands of 10° – 20° S (tropical, regions 1–3 in Figure 1), 20° – 30° S (subtropical, regions 4–6), and 30° – 40° S (temperate, regions 7–9). To investigate possible longitudinal variations, these latitudinal bands have been subdivided into three longitudinal zones covering 110° – 130° E, 130° – 140° E and 140° – 155° E respectively. Results of a cluster analysis of rainfall events by *Drosowsky* [1993] have implied the usefulness of a longitudinal division. Only data over land has been used in the analysis. Figure 1

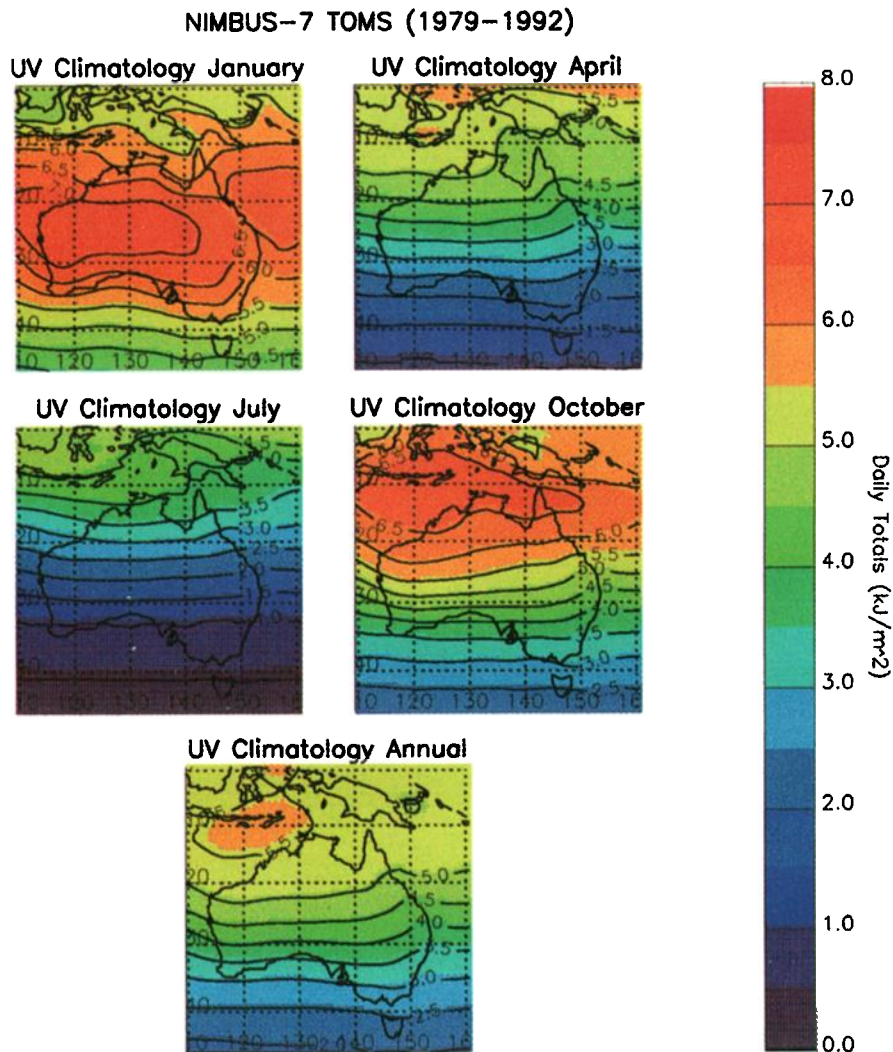


Plate 1. Climatology of daily integrated erythemal UVR exposures from TOMS over the Australian continent for January, April, July, October, and the annual average.

shows the location of these regions and their relation to the state boundaries.

3.2. Climatological Averages and Seasonal Cycles

Figure 5 shows the seasonal cycle for erythemal UVR exposure (top), total ozone (middle), and cloud cover (bottom) for the nine regions on the Australian mainland, the three latitudinal zones labeled tropical, subtropical, and extratropical, the island of Tasmania, and the entire Australian continent. These climatological seasonal cycles were derived from 14 years of monthly averaged time series. Differences in line style specify the longitudinal subregions. Dotted lines represent the most western region (1, 4, and 7; see Figure 1), the dashed lines denote the central regions (2, 5, and 8) and the dashed-dotted lines represent the eastern regions (3, 6, and 9). Table 4 summarizes the corresponding annual averages as well as minimum and maximum monthly averages.

3.2.1. UV radiation. The seasonal variation in erythemal UVR is predominantly influenced by changes in the maximum solar elevation at any given location over the course of a year. For example, when the seasonal variation of the UVR exposures is expressed as a linear function of the noon solar elevation, the variance of seasonal cycle of UV radiation is explained by $r^2 = 95\%$. (The term “explained variance” is defined as the square of the correlation coefficient.) Outside the tropical belt the Sun reaches its highest elevations in December and the lowest in June. Within the tropical region the UV radiation stays fairly constant between November and February, when the noon solar elevation reaches its maximum values. The tropical part of Australia receives the highest amount of the erythemal UVR exposure, 5.3 kJ m^{-2} as an annual average (see Table 4). The exposures in the subtropical region, 4.6 kJ m^{-2} , are twice as high as the exposures in Tasmania, 2.3 kJ m^{-2} . The extratropical region receives 64% of the amount of the tropics. Averaged over the

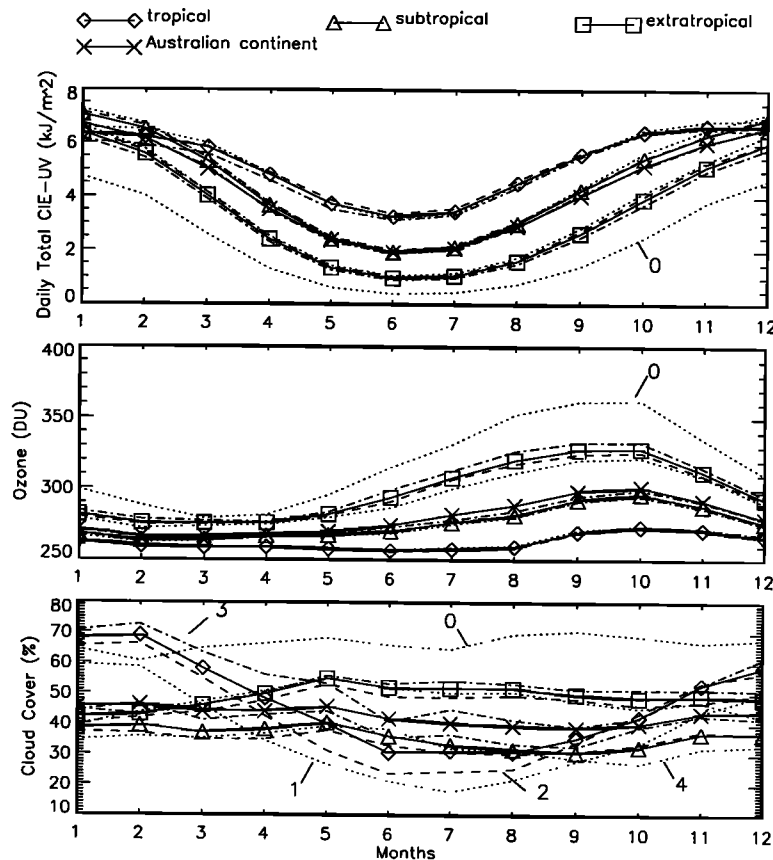


Figure 5. Climatological seasonal cycle of erythemal UVR exposure, total ozone, and cloud cover for selected regions in Australia (see Figure 1) and the entire Australian continent derived from 14 years of TOMS data between 1979 and 1992. Symbols indicate the following regions: tropical (diamonds), subtropical (triangle), extratropical (squares), the island of Tasmania (0), and the entire Australian continent (crosses). Differences in line style specify the longitudinal subregions. Dotted lines represent the most western region (1, 4, and 7; see Figure 1), the dashed lines denote the central regions (2, 5, and 8), and the dashed dotted lines represent the eastern regions (3, 6, and 9).

year and for the entire Australian continent, daily exposures of 4.4 kJ m^{-2} are obtained, which are comparable to the average amount received in the subtropical region. The latitudinal gradient of the annual averaged UVR exposures is about $1 \text{ kJ m}^{-2} (10^\circ \text{ latitude})^{-1}$. As Figure 5 and Table 4 indicate, in the summer months, exposures in the extratropical regions are as large as in the tropics. Considerable latitudinal differences exist in winter, that is, 0.9 kJ m^{-2} between the extratropics and subtropics, and 1.4 kJ m^{-2} between the subtropics and tropics. Table 4 shows that the longitudinal variability can be as large as 0.3 kJ m^{-2} , that is, about 5–9% of the average in the respective latitude belt of Australia.

3.2.2. Ozone. It is apparent that the seasonal variability of ozone (middle plot of Figure 5) increases from the tropics toward Tasmania. This distribution reflects the transport of ozone from the equator to higher latitudes. Ozone is produced photochemically in the tropical stratosphere with maximum molecular concentrations at a height of 22 km and maximum mixing ratio near 35 km. As a result of the Brewer-Dobson circula-

tion [Andrews *et al.*, 1987], ozone is transported from the source region poleward. It is advected from the tropical source region into higher latitudes by the wave-driven extratropical pump [Holton *et al.*, 1995], where it enters a zone of large-scale subsidence. In the Southern Hemisphere the highest ozone values occur in springtime in the subpolar region. There is little seasonal variation in the tropics. A springtime peak in ozone can be observed in all regions outside the tropics, which results from a dynamically and radiatively driven peak in the Brewer-Dobson circulation at this time [Andrews *et al.*, 1987; Atkinson, 1996].

3.2.3. Cloud cover. The cloud cover variability does not show a pronounced seasonal cycle for most regions outside the tropics. In the tropical regions (denoted 1–3 in Figure 5) the monsoon affects the seasonal cycle. Cloud cover increases steadily from August to February, the buildup and duration of the monsoon season. The subtropical regions show a slight seasonal cycle with a minimum in spring. The extratropical regions show an increase of cloud cover in late fall (May) and a

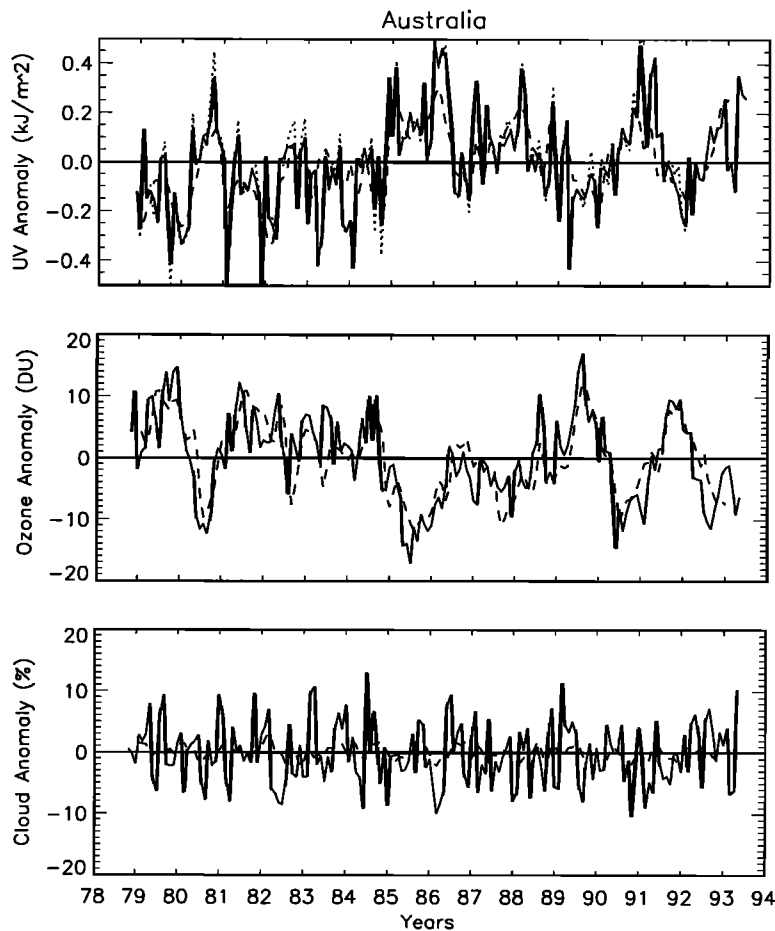


Figure 6. Deseasonalized time series of TOMS (top) erythemal UVR, (middle) ozone, and (bottom) cloud cover for the Australian region. The dotted line in the top diagram shows the linear regression fit of erythemal UVR changes as a function of changes in ozone and cloud cover (see Table 5). The dashed lines show the regression time series derived from a fit of equation (3).

slow decline in the rest of the year with a minimum in January.

4. Analysis

The climatological seasonal cycle is subtracted from the time series, and a detailed analysis of the time series anomalies is carried out. The correlations between the anomalies of UVR exposures, ozone, and cloud cover (derived from the three TOMS data sets described earlier) are discussed, and, finally, a trend analysis is performed. The trend analysis includes several statistical proxies for expected interannual signal components, which are described in detail. The seasonal dependence, the annual averages, and the statistical significance of the results will be presented.

4.1. Sensitivity of UVR Anomalies to Ozone and Cloud Cover Changes

It is investigated whether the temporal variability of the UVR exposure anomalies can be described as a linear function of ozone and cloud cover anomalies. Deseasonalized time series have been calculated for each

parameter and region. Figure 6 shows the deseasonalized time series of UVR (top), ozone (middle) and cloud cover (bottom) derived from TOMS data for the entire Australian continent as an example. The seasonal signal in the time series has been eliminated by subtracting the climatological monthly averages (see Figure 5) from the monthly mean time series (not shown). The dashed lines show results of a modeled time series using a regression model that will be discussed in section 4.2. The dotted line in the UV plot represents the fitted UVR anomalies as a linear function of ozone and cloud cover anomalies (see Table 5). The dotted line matches the deseasonalized time series closely, thus indicating that the UVR exposure anomalies can be approximated as a linear function of ozone and cloud cover anomalies. The linear model explains 99% of the variance of the observed UVR anomalies. The statistical results for the other Australian regions are summarized in Table 5. A close relationship between the TOMS UVR exposure anomalies, TOMS ozone, and TOMS-derived cloud cover anomalies is expected to some extent. As discussed earlier, UVR exposures have been derived from a radiative transfer model as a nonlin-

Table 4. Annual Averages, Minima, and Maxima of UVR, Ozone, and Cloud Cover Derived From TOMS Data Between 1979 and 1992

Region	UV, kJ m^{-2}			Ozone, DU			Cloud Cover, %		
	Mean	Min	Max	Mean	Min	Max	Mean	Min	Max
Tropical	5.3 ± 1.3	3.3	6.7	263 ± 6	256	273	47.1 ± 14.1	30.6	69.0
1	5.4 ± 1.4	3.2	6.9	263 ± 6	257	274	36.7 ± 14.6	17.7	59.3
2	5.3 ± 1.2	3.4	6.7	262 ± 6	256	272	43.5 ± 15.8	23.6	66.2
3	5.1 ± 1.3	3.1	6.6	263 ± 6	257	274	53.2 ± 11.8	39.2	72.5
Subtropical	4.6 ± 1.9	1.9	7.0	276 ± 12	263	296	36.0 ± 3.2	30.6	40.4
4	4.7 ± 2.0	1.9	7.2	275 ± 11	262	295	33.7 ± 3.7	27.0	39.3
5	4.6 ± 1.9	2.0	7.1	275 ± 11	263	295	34.5 ± 2.8	30.1	37.8
6	4.4 ± 1.8	1.9	6.7	278 ± 12	265	300	40.1 ± 4.6	32.6	46.5
Extratropical	3.4 ± 2.0	1.0	6.4	298 ± 21	276	329	49.0 ± 3.7	42.0	54.9
7	3.6 ± 2.1	1.1	6.6	293 ± 19	272	322	47.6 ± 4.4	39.3	55.1
8	3.5 ± 2.0	1.0	6.5	296 ± 20	275	326	47.1 ± 3.6	40.0	53.0
9	3.3 ± 2.0	0.9	6.2	301 ± 22	276	333	50.5 ± 3.9	43.1	55.8
Tasmania	2.3 ± 1.7	0.4	4.7	318 ± 30	279	362	66.5 ± 2.8	60.4	70.6
Australia	4.4 ± 1.8	1.9	6.7	280 ± 13	266	301	42.8 ± 2.6	38.8	46.3

Here, kJ m^{-2} = kilo Joules per square meters; DU, Dobson units.

ear function of ozone and cloudiness (see section 2.1.2). Moreover, TOMS ozone data have been used as input to the UVR exposure algorithm; however, the TOMS partial cloud reflectivities have not. Under these conditions it is remarkable that the UV anomalies in a given region can be almost entirely reconstructed as a linear combination of the ozone and cloud cover anomalies.

Table 5 includes further details of the regression analysis. The linear regression coefficients a_1 describe the sensitivity of UVR changes due to ozone changes. This coefficient can be related to the linear radiation amplification factor (RAF), which is defined as $\Delta\text{UV}/\text{UV} = -\text{RAF}(\Delta O_3/O_3)$ [e.g., *McKenzie et al.*, 1991]. The

RAF is a function of solar zenith angle. Although the radiation amplification factor is defined to describe changes in UV irradiances, here the same concept is applied for the daily integrated exposures. *McKenzie et al.* [1991] found that ozone reductions of 1% cause an increase in the erythemal UV irradiance of $1.25 \pm 0.20\%$ at Lauder, New Zealand (45°S). The regression coefficients derived here, that is, $a_1 = -\text{RAF}_{\text{exposures}}$, vary between -0.95 in the tropics to -1.3 in the extratropics (35°S). For Australia the average value of $a_1 = -1.26$ is very close to the value for the irradiance measurements obtained by *McKenzie et al.* [1991].

The effect of cloud variability on UV radiation expo-

Table 5. Results of the Linear Regression of Relative UVR Erythemal Exposure Anomalies as a Function of Relative Anomalies in Ozone and Cloud Cover Based on TOMS Data

Region	Ozone		Clouds		r_{fit}
	$(a_1 \pm \sigma)$	r	$(a_2 \pm \sigma)$	r	
Tropical	-1.11 ± 0.10	-0.40	-0.31 ± 0.02	-0.80	0.98
1	-0.92 ± 0.10	-0.46	-0.24 ± 0.01	-0.90	0.99
2	-1.09 ± 0.17	-0.34	-0.31 ± 0.03	-0.83	0.97
3	-0.95 ± 0.22	-0.31	-0.35 ± 0.04	-0.83	0.94
Subtropical	-1.21 ± 0.03	-0.89	-0.23 ± 0.01	-0.69	1.00
4	-1.20 ± 0.03	-0.88	-0.19 ± 0.01	-0.86	1.00
5	-1.20 ± 0.03	-0.82	-0.22 ± 0.01	-0.63	1.00
6	-1.24 ± 0.03	-0.81	-0.26 ± 0.01	-0.42	1.00
Extratropical	-1.30 ± 0.04	-0.50	-0.30 ± 0.01	-0.70	1.00
7	-1.30 ± 0.04	-0.61	-0.25 ± 0.01	-0.77	1.00
8	-1.27 ± 0.04	-0.52	-0.28 ± 0.01	-0.74	1.00
9	-1.27 ± 0.05	-0.44	-0.33 ± 0.01	-0.78	1.00
Tasmania	-1.12 ± 0.08	-0.34	-0.47 ± 0.02	-0.80	0.99
Australia	-1.26 ± 0.04	-0.79	-0.28 ± 0.01	-0.46	1.00

$\Delta\text{UV} = a_1 \cdot \Delta\text{ozone} + a_2 \cdot \Delta\text{clouds}$; r , partial correlation coefficient; r_{fit} , correlation coefficient of the regression fit.

sures is more complex. The regression coefficients a_2 in Table 5 seem to indicate a longitudinal dependence of the sensitivity of UVR exposure to cloud cover changes. The cloud cover changes are more effective in the western part of Australia in comparison to the eastern part. In the subtropics a 10% decrease in cloud cover would increase the UV radiation between 1.9 and 2.6%. In the tropics a 10% decrease in cloud cover would result in a 2.4% increase of UVR at the west coast but a 3.5% increase at the east coast. This is comparable to the 2.5-3.3% increase in the extratropics. Several reasons might explain the longitudinal dependence: a change in surface reflectivity due to a change in vegetation, variations in terrain height, and a change in cloud type. Convective cloud types are predominant at the coast east of the Great Dividing Range [Warren *et al.*, 1986], an area characterized by forests and farm lands, whereas altostratus prevails in the western and central parts of Australia over the desert. Cloud cover in the arid subtropics is characterized predominantly by altostratus and cirrus. In the extratropics the most frequent cloud types are stratus and cirrus over forests and farmland. The sensitivity of the UVR exposures to changes in cloud cover is largest in Tasmania, where stratocumuli are the most frequent cloud type. Generally, the UVR exposures are more sensitive to changes in cloud cover in vegetated areas, where convective clouds are dominant. Averaged over the Australian continent, an increase in cloud cover of 10% will reduce the daily UVR exposure by 2.8%. These results are within the range of values of 1.2-6.4% per 10% cloud cover change that was derived from measurements at several stations in the United States [Frederick and Snell, 1990].

While the correlation between ozone and UVR anomalies is quite high in most parts of Australia, it is interesting to note that outside the tropics the ozone-UVR correlation coefficient is lowest in Tasmania. It has been expected that the detection of the effects of the ozone depletion on the surface UV radiation would most likely be at higher latitudes, which are associated with a larger magnitude in ozone fluctuations. However, these regions also have a large amount of cloud cover (66% for Tasmania; see Figure 5) and cloud variations throughout the year. The analysis shows that ozone variations affect climatological changes of erythemal UVR exposures far less than variabilities in cloudiness.

4.2. Trend Analysis

Previous studies have indicated that the 11 year solar cycle, the quasi-biennial oscillation (QBO) in zonal wind strength in the lower stratosphere, and the El Niño-Southern Oscillation (ENSO) affect the ozone distribution [Stolarski *et al.*, 1991; Randel and Cobb, 1994]. A regression model that takes into account these signal components has been described by Randel and Cobb [1994]. It is based upon the regression model for ozone introduced by Stolarski *et al.* [1991] with an additional ENSO term to account for the ENSO signal that has

been found in the total ozone field by Shiotani [1992]. The regression equation used to model the UVR, ozone, and cloud cover anomalies reads

$$\begin{Bmatrix} \Delta UV(t) \\ \Delta O3(t) \\ \Delta C(t) \end{Bmatrix} = \alpha \cdot s_1(t) + \beta \cdot s_2(t) + \gamma \cdot s_3(t) + \epsilon \cdot s_4(t) + \text{residual}, \quad (3)$$

where s_1 , s_2 , s_3 , and s_4 are the trend, solar, QBO, and ENSO signal components. All regression coefficients α , β , γ , and ϵ in (3) have the form $\alpha = A_1 + A_2 \cos \omega t + A_3 \sin \omega t + A_4 \cos 2\omega t + A_5 \sin 2\omega t + A_6 \cos 3\omega t + A_7 \sin 3\omega t$, with $\omega = 2\pi/12 \text{ months}^{-1}$ to take into account seasonal variability. Each term in (3) thus has seven parameters to be determined simultaneously. To approximate the solar signal s_2 , the 10.7 cm (or 2800 MHz) solar radio flux is used. Data have been obtained from the National Geophysical Data Center and are based on the radio telescope measurements in Ottawa (prior to June 1991) and Penticton, British Columbia, after June 1991. Units of the 10.7 cm solar flux are given in $10^{-22} \text{ W m}^{-2} (\text{Hz})^{-1}$ (or 10^4 Janskys) and frequently referred to as F10.7cm, which will be used hereafter. The zonal wind monthly anomalies at 30 mbar in m s^{-1} (s_3) have been used to take into account the QBO effect. The zonal wind data have been provided by the Free University Berlin. The Southern Oscillation Index (SOI), that is, the normalized pressure difference between Tahiti and Darwin (s_4), has been obtained from the National Oceanic and Atmospheric Administration (NOAA) Climate Prediction Center. Figure 2 of Randel and Cobb [1994] shows these data sets for the period between 1979 and 1992.

4.3. Seasonal Dependencies of the Signal Components

The coefficients (α , β , γ , and ϵ) have been estimated for each individual month from (3) (see Randel and Cobb [1994] for a more detailed discussion of the fitting procedure) with a least squares fit routine from the linear algebra package LAPACK [Anderson *et al.*, 1992]. Figures 7-11 show the seasonal variation of the coefficients. In each, the top diagram shows the UVR, the middle diagram the ozone, and the bottom diagram the cloud estimates. In order to compare the results, an understanding of the typical fluctuations of the different signal components is required. From Figure 2 of Randel and Cobb [1994] (which shows the different signal components over the 14 year period) it is evident that the difference between maximum and minimum solar flux is typically about 100 F10.7cm within a time interval of 5.5 years (1/2 the solar cycle). The coefficient for the solar signal, β , thus describes the response of UVR, ozone, and cloud cover due to a typical change in solar flux between solar maximum and solar minimum. On the other hand, the results for the QBO in Figure 9 are given in terms of a typical amplitude of the zonal wind fluctuation. To express the UVR, ozone, and

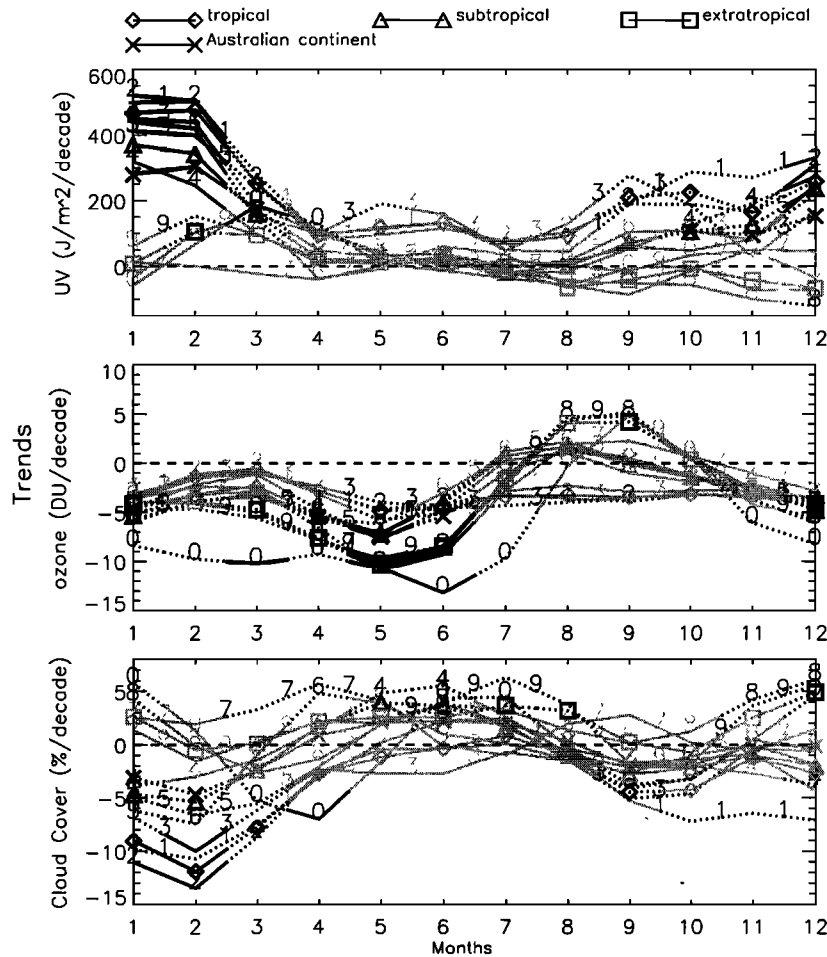


Figure 7. Trends (i.e., coefficient α in equation (3)) in erythemal UVR ($\text{J m}^{-2} \text{decade}^{-1}$), ozone (DU decade^{-1}), and cloud cover ($\%$ cloud amount per decade) for selected geographical regions of Australia (see Figure 1) and for the entire Australian continent derived from TOMS data. Statistically significant results on the 2σ level are shown as black solid lines; signals above the σ level are shown as black dashed lines. Light gray values indicate no statistical significance of the results. Refer to the discussion in text for further details.

cloud cover variation in terms of the difference between the maximum and minimum zonal wind, that is, the westerly and easterly phase of the QBO, the results for γ in Figure 9 should be multiplied by a factor of 2, because the 30 mbar zonal wind typically varies between -20 and $+20 \text{ m s}^{-1}$ within 2 years. Figure 11 shows the coefficients ϵ of the ENSO variations with respect to the standard deviation of the normalized SOI ($1 \text{ normalized SOI} = 1 \text{ SOI}/\sigma_{\text{SOI}}$). The SOI typically would vary by about 2 standard deviations between average El Niño and La Niña events. Again, to express the UVR, ozone, and cloud cover signal in terms of the difference between maximum and minimum signal, the values in Figure 11 should be multiplied by a factor 2. Variations in SOI are associated on timescales of 2-5 years. It should be kept in mind that the signal components interfere with each other on different time scales, 11 years for the solar cycle, quasi-biennial for the QBO, and 2-5 years for ENSO.

The different shadings in Figures 7 -11 indicate the levels of significance of the results, which have been determined by comparing each signal to its standard deviation σ . Solid black lines indicate that the result is significant on the 2σ level, which corresponds to a confidence interval of 95% [Bloomfield *et al.*, 1988]. Dashed lines indicate that the signal is larger than the standard deviation, whereas light gray values indicate that the results are not statistically significant. In the following the term “significant” is used to characterize the signals that exceed the 2σ level.

4.3.1. Trend component. Figure 7 shows the trends α in absolute units, and Figure 8 shows the trends in relative units. Each line is labeled with either a number identifying the region, as defined in Figure 1, or a symbol for an entire latitudinal zone, as explained in the top portion. Tasmania is labeled “0.” It is apparent that the trend components are significant during the summer months (December/January/February) in

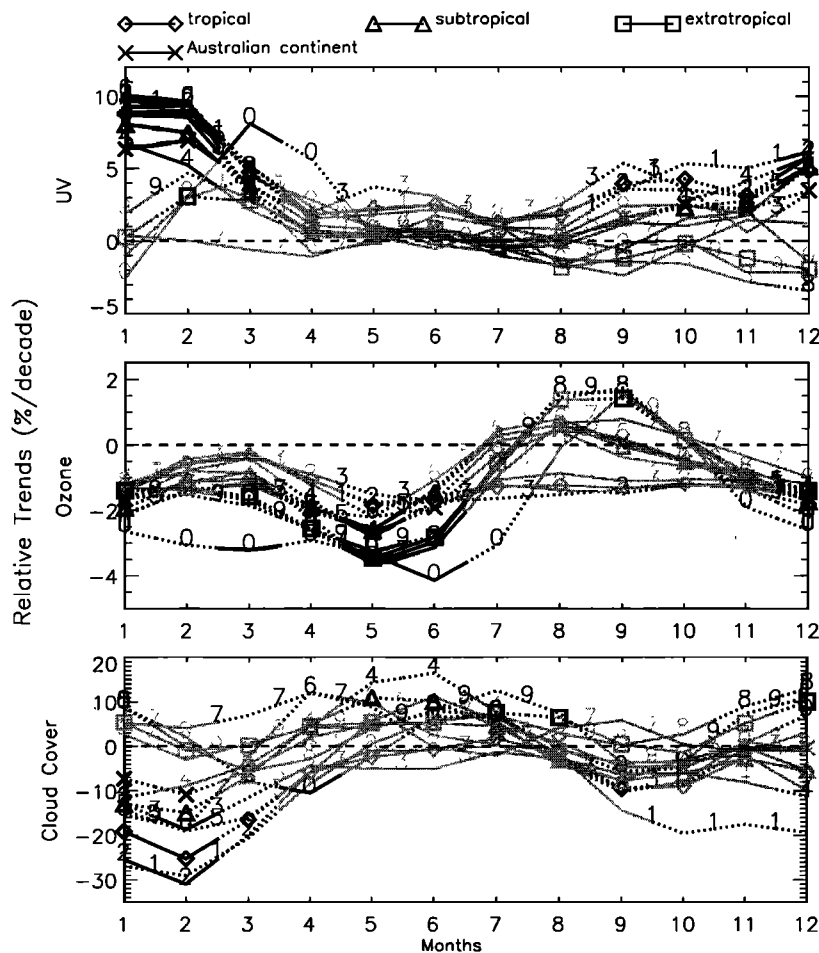


Figure 8. Same as Figure 7 except that trends are given as percent changes per decade. Percent changes have been calculated with respect to the climatological averages of UVR, ozone, and cloud cover (see Table 4).

all regions except the extratropics. The magnitudes of the UVR trends reach their absolute maxima of approximately 0.3 and $0.5 \text{ kJ m}^{-2} \text{ decade}^{-1}$ (Figure 7), which correspond to relative values of about $5\text{--}10\% \text{ decade}^{-1}$ (Figure 8). It should be noted that the UVR trends in the summer months are statistically significant in regions where ozone and cloud cover trends are in phase and declining. As ozone and cloud cover decreases are anticorrelated with UV anomalies, both atmospheric parameters contribute to an increase in UVR exposures.

It is surprising that UVR trends are statistically significant in tropical regions rather than in the regions at the extratropics. *Lubin and Jensen [1995]* predicted increases in solar-noon UVR values at higher latitudes in the summer months, but the results from this analysis indicate no evidence for such an increase.

Although the ozone depletion is statistically significant in the fall with values of $5\text{--}15 \text{ DU decade}^{-1}$ ($2\text{--}4\% \text{ decade}^{-1}$) (May), trends in cloud cover are not statistically significant; neither are the UVR exposures. In spring the ozone depletion is small or nonexistent. This

is consistent with results from zonally averaged ozone trends [see *Randel and Cobb, 1994, Figure 5*].

Trends in cloud cover are generally negative over the Australian region in the summer months and positive in the winter months. Cloud cover trends are statistically significant only in February in the central and eastern parts of the tropical region. This might indicate that cloud cover at the end of the monsoon season has decreased significantly in the period of 1979–1992. Another explanation might be the spatial variation of the moving cloud lines, associated with the monsoon shear line. The monsoon shear line shows considerable spatial and temporal variability, as discussed in numerous studies [*Suppiah, 1992; McBride and Keenan, 1982; Drosowsky and Holland, 1987; Drosowsky et al., 1989; Drosowsky, 1996*]. Interannual variability of the monsoon duration and rainfall have been reported [*Suppiah, 1992; Drosowsky, 1996*]. Further work is needed to understand the interactions between Australian monsoon and longer-term variations [*Drosowsky, 1996*]. The duration of this data set of 14 years is too short to address

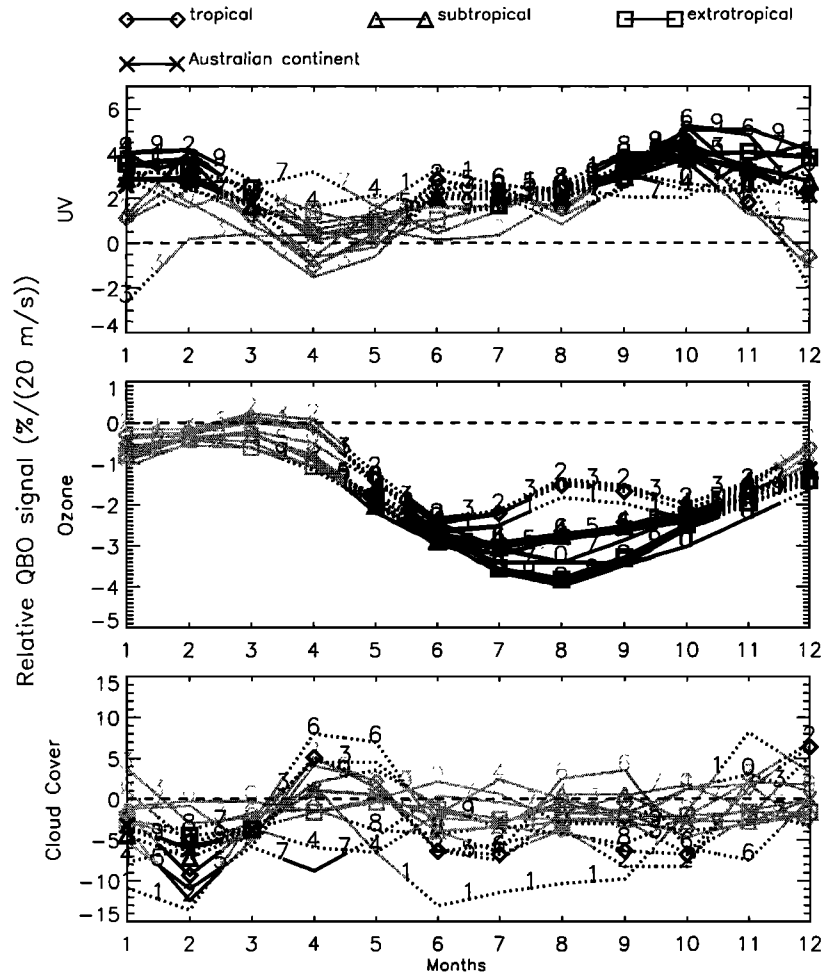


Figure 9. Relative contribution of the quasi-biennial oscillation (QBO) on the erythemal UVR, ozone, and cloud cover (i.e., coefficient γ in equation (3)) for eight regions of Australia and for the entire Australian continent derived from TOMS data. The QBO-associated regression fits are given in units of percent per 20 m s^{-1} change in the 30 mbar zonal wind strength. Statistically significant results on the 2σ level are shown as black solid lines; signals above the σ level are shown as black dashed lines. Light grey values indicate no statistical significance of the results. The magnitude of 20 m s^{-1} is approximately the amplitude of the zonal wind change during a QBO. To estimate the maximum relative change in UVR, ozone, and cloud cover as would be observed between the westerly (positive) and easterly (negative) phase QBO, the results should be multiplied by a factor of 2.

this problem, as inter-decadal climate variabilities cannot be resolved.

4.3.2. QBO signal. Figure 9 shows that the QBO signal leads to a reduction of ozone in all regions in Australia. Ozone is reduced by 1-4% if the zonal wind strength increases by 20 m s^{-1} . This reduction is significant between April and December with a maximum signal in the wintertime. This finding is consistent with the results of *Yang and Tung [1995]*. Their study showed that QBO ozone signal at higher latitudes is out of phase with the equatorial QBO signal of ozone, with a strong signal in the winter-spring season. Ozone in the equatorial region was found to be leading the Singapore wind by 1-2 months [*Tung and Yang, 1994a, b*]. Furthermore, a change of phase was found to occur at

about 12° latitude and lasts to about 16° - 17°S [see *Yang and Tung, 1995, Figure 5*]. This phase shift is evident in Figure 9, because in the tropical regions of Australia, which cover the latitudes between 12° and 20°S (labeled 1-3 and with diamonds), the negative effect of the QBO on the ozone occurs 2 months earlier than in all other regions. The QBO has little effect on changes in cloud cover, except for the tropical and subtropical regions in February. A statistically significant positive signal in UVR exposures of about 3-4% per 20 m s^{-1} occurs in the summer months. It is out of phase with the negative QBO signal in ozone, but occurs when ozone and cloud cover signals are in phase.

4.3.3. Solar signal. Figure 10 shows the effect of the solar signal on the UVR, ozone, and cloud cover.

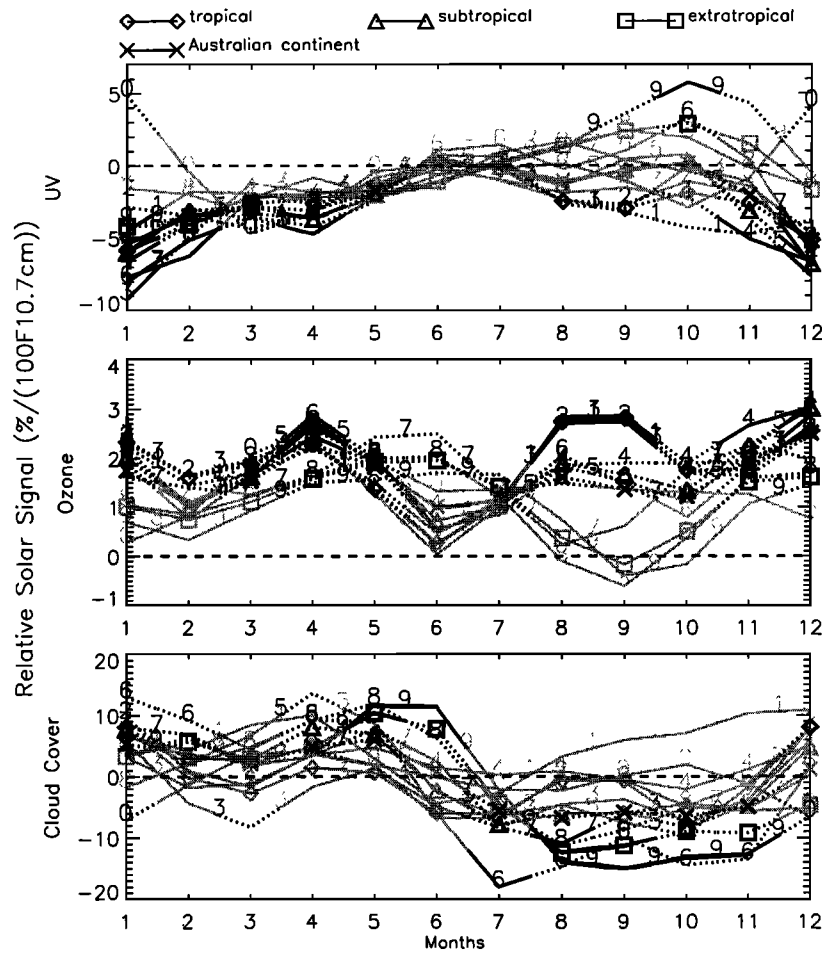


Figure 10. Relative contribution of the variability in solar radio flux on the erythemal UVR, ozone, and cloud cover (i.e., coefficient β in equation (3)) for eight regions of Australia and for the entire Australian continent derived from TOMS data. The solar cycle regression fits are given in percent per 100 F10.7cm flux, which is the typical change in magnitude between solar minimum and solar maximum. Statistically significant results on the 2σ level are shown as black solid lines; signals above the σ level are shown as black dashed lines. Light gray values indicate no statistical significance of the results.

An increase in solar radio flux by 100 F10.7cm seems to result in positive ozone anomalies of 1-3% throughout the year. Changes in solar flux are associated with significant changes in the total ozone during late fall and early spring. UVR levels are reduced significantly in the summer months in tropical and subtropical regions between 5 and 10% per solar flux increase of 100 F10.7cm.

Results also indicate a negative cloud cover signal in the southeastern part of Australia (regions 6 and 9) during winter and spring (August-October) and a positive signal in the fall (May-June). It has been shown recently that changes in solar flux might be associated with changes in cloud cover. *Svensmark and Friis-Christensen* [1997] showed a strong correlation between total cloud cover and cosmic ray flux. Cosmic ray flux is anticorrelated with the solar flux. Their finding suggests that the cloud cover is anticorrelated with the

solar cycle, with cloud cover variations of 3-4% during one cycle. Figure 10 suggests a statistically significant anticorrelation in the extratropics in winter and spring. However, in late fall and early winter, cloud cover and solar cycle seem to be positively correlated in the same regions. The seasonality of the results might be associated with a simultaneous change of cloud cover and cloud opacity. For example, *Kuang et al.* [1998] reported an anticorrelation of cloud cover with the solar cycle and a positive correlation of the mean cloud optical thickness. They speculated that the reason might be an increase of the thin clouds along with the decrease of thick clouds during solar minimum. A physical mechanism was proposed by *Tinsley* [1996], who related the solar cycle to changes in the air-Earth current density due to external modulation of the electric circuit by the solar wind. He suggests that electrostatic charge accumulation on supercooled droplets and aerosols near

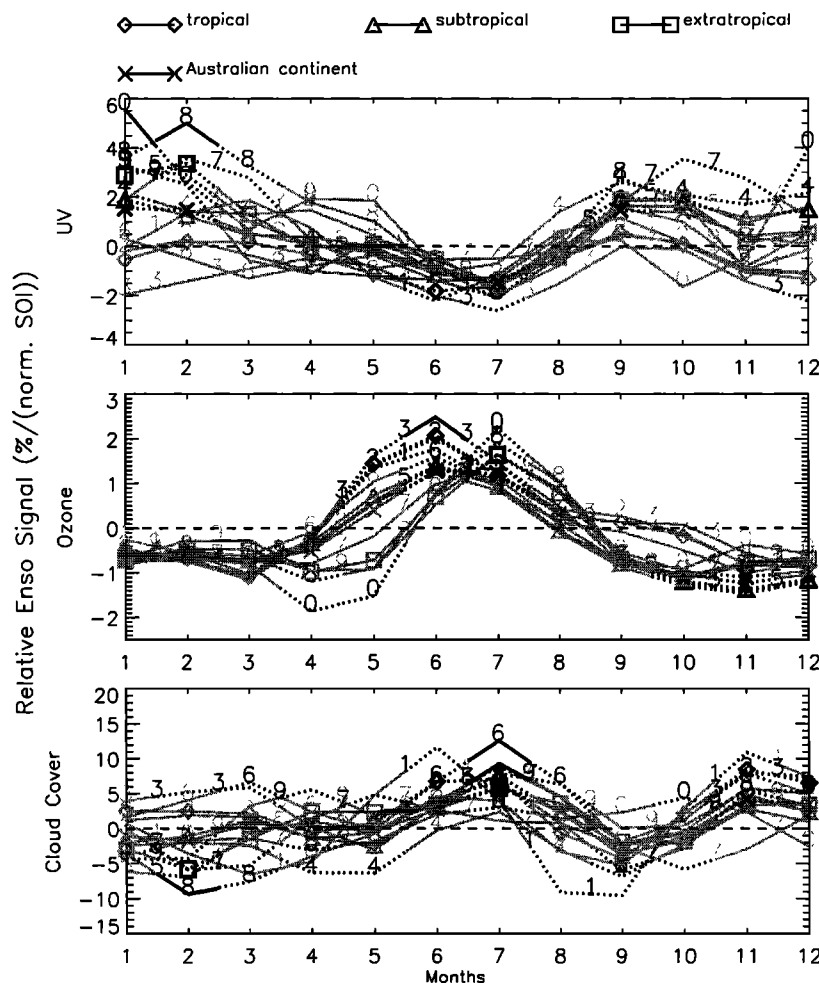


Figure 11. Relative contribution of the ENSO variability described by the Southern Oscillation Index (SOI) on erythemal UVR, ozone, and cloud cover (i.e., coefficient ϵ in equation (3)) for eight regions of Australia and for the entire Australian continent derived from TOMS data. The ENSO regression fits are given in percent per normalized SOI (1 normalized SOI = SOI/σ_{SOI}). Statistically significant results on the 2σ level are shown as black solid lines; signals above the σ level are shown as black dashed lines. Light gray values indicate no statistical significance of the results. Multiplying the results with a factor of 2 would give an estimate of the maximum change in UVR, ozone, and cloud cover, corresponding to a change of 2 standard deviations in SOI.

cloud tops affects the probability of ice nucleation and droplet freezing. For light cloud cover this increase in ice nucleation can reduce cloud opacity and albedo, but for storm cloud systems the effect is found to intensify the storm. The downward current intensity varies as a function of latitude and increases toward higher latitudes. This is consistent with the results in Figure 10, where highest levels of confidence for cloud cover changes due to a change in solar cycle are found in the extratropical regions. However, despite some evidence for a relationship between cloud cover and solar cycle, the results are far from conclusive.

4.3.4. ENSO signal. Figure 11 shows the contribution of the ENSO signals to the different time series. An El Niño or ENSO warm event is characterized by negative SOI. Statistically significant positive signals in

UVR are observed during the summer months in the central and western part of Australia. These are associated with negative anomalies of the cloud cover signal. It appears that in winter during a change from El Niño to La Niña years (positive SOI), cloud cover will increase in the tropical and subtropical regions at the east coast (6 and 9) (Figure 11). This might be explained by the regions' closeness to the oceanic warm pool, where convection is intense. Figure 11 shows a significant positive signal in cloud cover in the subtropical and extratropical eastern regions of the continent in July. This is consistent with the results of *McBride and Nicholls* [1983], who showed correlations between SOI and rainfall in the southeastern part in the summer months. However, they also reported extensive spatial correlations in September–November between rain-

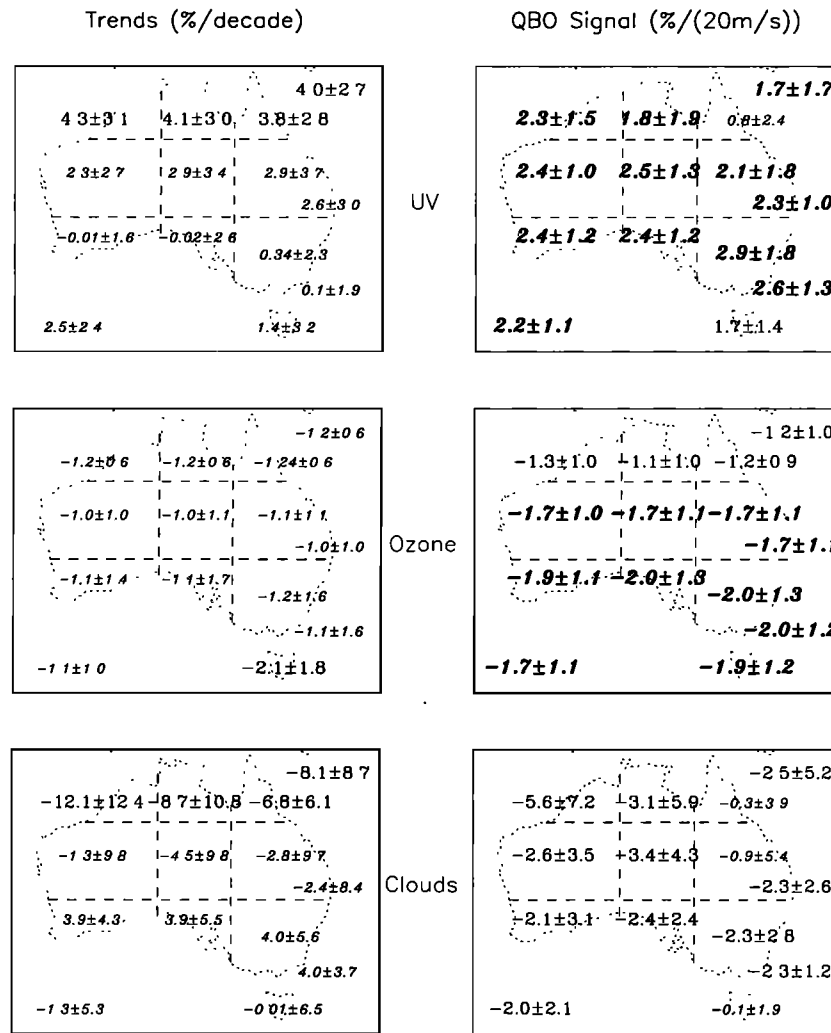


Figure 12. Annually averaged trend and QBO-associated regression coefficients and standard deviations. The left column shows the trend estimates for (top) UVR, (middle) ozone, and (bottom) cloud cover. The right column shows the QBO regression fit for each variable. Each value represents the result for one region as defined in Figure 1. Values on the right-hand side represent the result for the latitudinal band of the Australian continent (tropics, subtropics, extratropics). The value at the lower right is representative for Tasmania, and the value on the lower left is the signal representing the entire Australian continent, including Tasmania. Units are given in % per signal, where % refers to the percentage change of each variable (UVR, ozone, or cloud cover derived from TOMS data) with respect to its climatological average listed in Table 4. Trends are expressed in % per decade and the QBO signals are expressed in % per 20 m s⁻¹. The statistical significance of the results as estimated with the Monte Carlo method is indicated with different font styles. Small italic fonts indicate that results are not statistically significant. Estimates with confidence levels between 80 and 90% are indicated as roman fonts. Large bold italic fonts indicate estimates with confidence levels > 90%.

fall and SOI, which have not been found in the cloud cover changes here.

Statistically significant ozone signals of 2.5% per normalized SOI are observed in the tropics when the ENSO cycle changes from a La Niña event to an El Niño event. The result is consistent with the analysis of *Randel and Cobb [1994]*.

4.3.5. Annual averages. The results in Figures 7-11 have indicated strong seasonalities in the regres-

sion fits of the trend, QBO, solar, and ENSO signal components to the time series of UVR, ozone, and cloud cover. The next step is to examine whether these seasonal effects would result in a net annual effectiveness or cancel each other out. The regression fits for each month have been annually averaged, and the results plus standard deviations are shown in Figures 12 and 13. To elucidate the spatial distribution of the results, the annual averages have been printed on an Australian

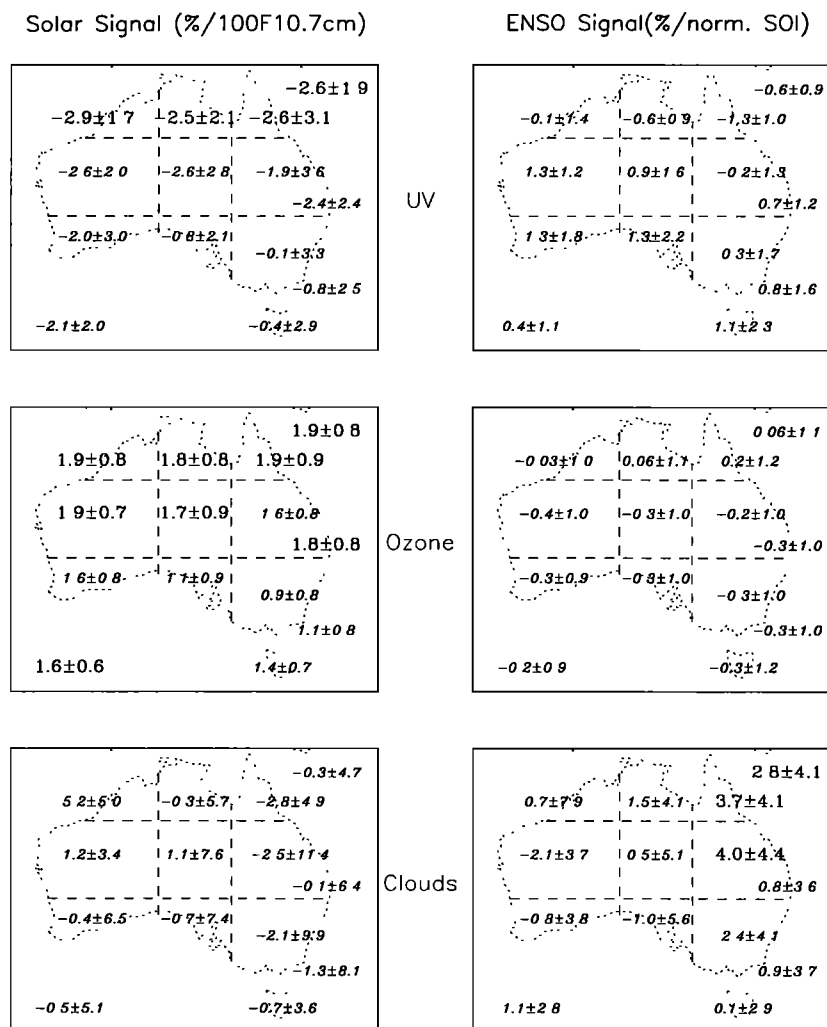


Figure 13. Annually averaged solar cycle and ENSO-associated regression coefficients and their standard deviations. The left column shows the solar cycle regression fit for (top) UVR, (middle) ozone, and (bottom) cloud cover. The right column shows the ENSO-associated regression fit for one region as defined in Figure 1. Values on the right-hand side represent the result for the latitudinal band of the Australian continent (tropics, subtropics, extratropics). The value at the lower right is representative for Tasmania, and the value on the lower left is the signal representing the entire Australian continent, including Tasmania. Units are given in % per signal, where % refers to the percentage change of each variable (UVR, ozone, or cloud cover derived from TOMS data) with respect to its climatological average listed in Table 4. The solar signal components are expressed in % per 100 F10.7cm and the ENSO signals are expressed in % per normalized SOI. The statistical significance of the results as estimated with the Monte Carlo method is indicated with different font styles. Small italic fonts indicate that results are not statistically significant. Estimates with confidence levels between 80 and 90% are indicated as roman fonts. Large bold italic fonts indicate estimates with confidence levels > 90%.

map. The boundaries of the regions for which the data are valid are indicated with dashed lines. Values plotted on the right-hand side of each map denote the longitudinal average of the three regions to their left. The value for Tasmania is plotted in the lower right. The average value for the entire continent is plotted in the lower left. All averages are expressed as relative changes with respect to their climatological averages stated in Table 4 and are given with their uncertainty σ . The uncer-

tainties have been calculated from the variances of the data. In addition, a TOMS instrument uncertainty of 1% has been taken into account [Herman et al., 1996]. Signals larger than the 2σ level are associated with confidence levels > 95%. Figure 12 shows that none of the estimates exceeds the 2σ level. This is in accordance with the results of Herman et al. [1996], who found that trends are not statistically significant at the 2σ level equatorward of 40° . Several estimates exceed the

1σ level. Their level of confidence is estimated with a bootstrap method as follows.

First, each of the original time series is divided into smaller portions consisting of 12 data points, which are then shuffled with the Monte Carlo method to reconstruct a new time series. This procedure is performed 100 times for each of the original UVR, ozone, and cloud cover time series. The results of the regression fits of these sample time series are compared to the original regression results. The confidence level of the regression fit of the original time series has been calculated from the number of estimates that exceeded the regression coefficient of the original time series. For example, if 20 estimates out of 100 exceeded the original fit, this resulted in a confidence level of 80%.

To distinguish between estimates with confidence levels $< 80\%$, confidence levels between 80 and 90%, and confidence levels $> 90\%$, the values in Figure 12 and Figure 13 have been printed using distinct fonts. Values indicating confidence level $< 80\%$ are shown in small italic letters, confidence levels between 80 and 90% are printed in slightly larger roman letters, and confidence levels $> 90\%$ appear as large, bold, italic letters.

It should be kept in mind that these confidence levels are not based on the uncertainties but on results from the bootstrap method. Figure 12 shows that annual trends in UVR, ozone, and cloud cover do not exceed the 2σ levels. However, annual UVR trends surpass the 1σ level uncertainty in the tropics and are associated with confidence level of 80-90%. Ozone trends with 80-90% confidence are observed only in Tasmania but are not associated with significant increases in UV.

Negative trends in cloud cover with confidence levels between 80 and 90% have been observed in the tropics. This is consistent with the findings of earlier studies. For example, although *Jones and Henderson-Sellers* [1992] reported an increase or no change in cloud cover between 1910 and 1989 for 318 stations in Australia, their data confirm a decrease in cloud cover from the end of the 1970s until 1989 [see *Jones and Henderson-Sellers*, 1992, Figure 1]. Furthermore, *Balling et al.* [1992] showed that from the late 1970s onward the maximum, minimum, and mean temperatures all rose sharply, indicating a discontinuity in the Australian temperature record. Subsequently, *Nicholls et al.* [1996] found that the relationship between temperature and rainfall changed in the late 1970s. They pointed out that an increase of Indian Ocean temperatures might be a causal factor for these changes. Although these studies were primarily concerned with climatic variables of temperature and rainfall, *Jones* [1991] pointed out that cloud cover is correlated negatively with the diurnal temperature range ($R=-0.87$) and the logarithm in rainfall ($R=0.75$), thus indicating that an anomalous change in cloud cover might also have occurred from the late 1970s to the early 1990s. Whether this change is due to a long-term trend or possible interdecadal variabilities is beyond the scope of this paper because it

cannot be resolved with the present data set. As the ozone trends are uniform across the continent, it seems the negative change in cloud cover is attributable to the positive trends in UVR in the tropics.

The QBO component appears to cause the dominant variations over the Australian continent. Statistically significant negative anomalies in the total column ozone over the Australian continent are associated with the westerly phase of the QBO. In addition, the cloud cover signal shows negative anomalies with confidence levels of 80%. Both the ozone and cloud cover decrease as a result of the westerly phase of the QBO. An increase in zonal wind strength of 20 m s^{-1} is associated with an increase of annual averaged UVR exposures of about 2.5%. A change in QBO from the easterly to the westerly phase is typically associated with a change in zonal wind strength of 40 m s^{-1} and thus can result in UVR increases of 5% for most of the Australian continent.

The solar signal produces changes in ozone in the tropical and subtropical regions which are associated with confidence levels between 80 and 90%. The surface UVR exposures are reduced by about 2% for an increase in solar flux by 100 F10.7cm, the typical change in solar flux between solar maximum and minimum. A possible influence of the solar cycle on cloud cover variation as discussed in section 4.3.3 is not evident in the annually averaged signal. This is consistent with the results of *Kuang et al.* [1998], who pointed out that the annually averaged TOMS reflectivities showed no change as a function of the solar cycle due to the compensating effect of cloud cover and opacity changes. However, further studies are required to address this problem.

Variations in ENSO cycle do not result in statistically significant changes of UV radiation and ozone. Cloud cover variations are not significantly affected for most of the Australian continent except for the regions in the northeast, where cloud cover increases can be observed with a confidence level of about 80-90%.

In essence, the QBO component is the only component that is associated with effective annual changes in UVR and ozone outside the tropics with confidence levels of 90% or higher. All other signal components are less effective. However, UVR trends in the tropics due to cloud cover changes and variations in tropical ozone, as well as UVR changes due to solar variations are still associated with confidence levels of 80%.

4.3.6. Regression fit. The dashed lines in Figure 6 show the fitted time series as obtained from (3). Correlation between the fitted UVR time series and the deseasonalized time series vary between 0.46 and 0.69. For ozone, correlations range from 0.72 to 0.83 and between 0.31 and 0.46 for cloud cover. It is perhaps not surprising that the correlation coefficients for the regression fits are small. This is particularly so in the UVR and cloud time series, which show a strong variability on timescales shorter than 4 months (see Figure 6). The parameterization in (3) can be sensitive only to frequencies as short as 3 year^{-1} . Generally, the

regression models explain between 20 and 48% of the variance of the UVR time series throughout the different regions with lowest values observed in midlatitudes. The ozone time series is modeled well, showing values of explained variance (square of the correlation coefficient) of 60-72%, consistent with findings of *Randel and Cobb* [1994] for the zonal averages. The model is less successful in accounting for the variance in the cloud time series. Here, values range from 10 to 24% depending on the region.

Standard deviations of the residuals between the regression fit and the original time series are about 4-7% for the UVR time series. For ozone the standard deviations of the residuals are between 2 and 3%, and for cloud cover they amount between 8 and 27%. Largest standard deviations in cloud cover are observed in the tropics.

5. Summary and Conclusions

The variability of UV radiation over the Australian continent and its dependence on the variability of ozone and cloud cover have been investigated using TOMS data sets. As a first step, the TOMS UVR exposures [*Herman et al.*, 1996] have been evaluated with surface measurements from broadband instruments, and good agreement has been found (Figure 2). TOMS partial cloud reflectivities have been used to estimate cloud cover by using relationships derived from intercomparison of surface cloud observations and overpass data at eight stations (Figures 3 and 4).

The Australian climatology of UVR exposures for 1979-1992 (Plate 1) has revealed a zonal asymmetry between the east coast and the rest of the continent, possibly associated with the differences of the vegetative humid climate east of the Great Dividing Range at the east coast and the arid climate in the central part. At any given location the seasonal cycle of UVR daily exposures varies primarily as a function of the noontime solar zenith angle. In summer the UVR exposures in extratropical regions of 6.4 kJ m^{-2} are almost as large as the maximum values of 6.7 kJ m^{-2} in the tropics. Annually averaged, the latitudinal gradient in UV radiation exposures is about $1 \text{ kJ m}^{-2} (10^\circ \text{ latitude})^{-1}$.

The TOMS UVR exposures, TOMS ozone, and cloud cover derived TOMS reflectivities have been spatially averaged to perform a statistical analysis for 10 individual regions, three latitudinal bands, and the entire continent of Australia (see Figure 1). Anomalies have been calculated by subtracting the climatological seasonal cycles (see Figure 5) from monthly averaged time series. It has been found that the deseasonalized UVR time series can be expressed as a linear function of ozone and cloud cover anomalies with $> 98\%$ of the variance explained. Trends and the regression coefficients of the quasi-biennial oscillation (QBO), the solar flux, and El Niño-Southern Oscillation (ENSO) cycle have been estimated for each individual month.

UV radiation trends of about $10\% \text{ decade}^{-1}$ have been obtained in the summer tropics, statistically significant on the 2σ level. These were associated with simultaneous depletion of ozone of $1\text{-}2\% \text{ decade}^{-1}$ and a decrease in cloud cover of $15\text{-}30\% \text{ decade}^{-1}$. Extratropical regions have not revealed significant UVR trends, most likely because of positive trends in cloud cover, which seem to counteract changes in the UV radiation due to ozone depletion. These results are interesting, as *Lubin and Jensen* [1995] predicted that in temperate regions "by the end of this century, trends in summer average local-noon UVR dose rates relevant to mammalian skin cancer or plant damage should be significant with respect to cloud variability.", (p. 710). Here, the analysis of the TOMS daily integrated UVR exposures shows that statistically significant summer UVR trends have been found in the tropics and not in the midlatitudes.

Annually averaged, the UVR trends were not statistically significant on a 2σ level (Figure 12). However, the UVR increases of about $4\% \text{ decade}^{-1}$ in the tropics have been associated with confidence levels between 80 and 90%. When comparing the trend estimates for ozone and cloud cover to the UVR trends, it has become evident that the UVR increases in the tropics could be related to decreases in cloud cover of $7\text{-}12\% \text{ decade}^{-1}$, because the ozone depletion has been uniform over the Australian continent at $1.1\% \text{ decade}^{-1}$. Ozone trends have not been found to be statistically significant. Only in Tasmania, ozone trends of about -2.1% per decade have been associated with confidence levels between 80 and 90%.

The ENSO cycle can lead to significant seasonal signals in sporadic regions (Figure 11). Statistically significant positive anomalies in cloud cover of 13% per normalized SOI have been observed in summer at the east coast. In the central extratropical region in summer the ENSO cycle is associated with a statistically significant negative anomaly in cloud cover of 10% per normalized SOI and a resulting positive anomaly in UVR of 5% per normalized SOI. Positive ozone anomalies of 2.5% per normalized SOI are observed during winter.

The QBO clearly dominates variations in the time series of ozone and UVR over the Australian continent (Figures 9 and 12). Ozone reductions of 1-4% per 20 m s^{-1} increase in zonal wind strength are observed between April and December with a maximum signal in winter. These ozone variations are out of phase with fluctuations in equatorial ozone, in accordance with the results discussed by *Yang and Tung* [1995]. Statistically significant increases in UVR exposures of about 3-4% per 20 m s^{-1} are apparent in the summer months. They are out of phase with the negative QBO signal in ozone, but occur when ozone and cloud cover signals are in phase (Figure 9). The westerly phase of the QBO is associated with statistically significant annual decreases in ozone of 1.7% per 20 m s^{-1} and increases in UVR exposures of 2.2% per 20 m s^{-1} (Figure 12).

The solar cycle has been associated with significant

reductions of UVR exposures of 5-10% per 100 F10.7cm in the tropical and subtropical regions in summer (Figure 10). A variation of 100 F10.7cm is typically observed between solar minimum and maximum. Annually averaged, a reduction of UVR levels in the tropics of 2.6% per 100 F10.7cm has been observed with confidence levels between 80 and 90% (Figure 13). The reductions in UVR exposures seem to be related to the increases in tropical ozone of 2% per 100 F10.7cm since annually averaged cloud cover changes were not significant.

The variations of the QBO and the solar cycle have a pronounced effect on the UV radiation in Australia. In addition, interdecadal variabilities or long-term trends in cloud cover can alter the amount of sunshine and thus the UV radiation at the surface. The results suggest that enhancements in UVR levels over the Australian continent might be expected during the summer months in years in which the QBO is in its westerly phase and the solar cycle is at its minimum. All signals combined might result in statistically significant increases in UVR during the summer months of 10-20% above the climatological average. It would be useful to monitor the QBO and solar cycle and predict seasonal UVR enhancements over Australia because of the potential adverse effects to human health and the effects on the natural UV photochemistry in the tropical troposphere, including the production/destruction of tropospheric ozone [Liu and Trainer, 1988]. Further studies are needed to address these questions.

Acknowledgments. The TOMS data sets were obtained from the NASA Goddard Space Flight Center. Special thanks go to Edward Celarier for the updated TOMS UV data set. Surface cloud observations were obtained from the National Climate Centre of the Bureau of Meteorology, Australia, with special thanks to Neil Plummer. We would like to thank Roger Atkinson, David Karoly, and the anonymous reviewers for their valuable comments and suggestions during the preparation this manuscript. This research was supported by the Cooperative Research Centres Program of the Australian Government.

References

- American Conference of Governmental Industrial Hygienists (ACGIH), Ultraviolet radiation, in *Documentation of the Threshold Limit Values*, pp. 471-474, Cincinnati, Ohio, 1980.
- Anderson, E., et al., *LAPACK User's Guide*, Soc. for Ind. and Appl. Math., Philadelphia, Pa., 1992.
- Andrews, D. G., J. R. Holton, and C. B. Leovy, *Middle Atmosphere Dynamics*, Academic, San Diego, Calif., 1987.
- Atkinson, R., Ozone variability over the southern hemisphere, *Cancer Forum*, 20, 168-173, 1996.
- Atkinson, R. J., and J. R. Easson, Reevaluation of the Australian total ozone data record, in *Ozone in the Atmosphere*, edited by R. D. Bojkov and P. Fabian, pp. 168-171, A. Deepak, Hampton, Va., 1989.
- Balling, R. C., S. B. Idso, and W. S. Hughes, Long-term and recent anomalous temperature changes in Australia, *Geophys. Res. Lett.*, 19, 2317-2320, 1992.
- Barton, I. J., The Australian UV-B Monitoring Network, *Tech. Pap. 46*, CSIRO Div. of Atmos. Phys., Aspendale, Victoria, Australia, 1983.
- Björn, L. O., Computer programs for estimating ultraviolet radiation in daylight, in *Radiation Measurement in Photobiology*, edited by B. L. Diffey, pp. 162-189, Academic, San Diego, Calif., 1989.
- Bloomfield, P., D. R. Brillinger, D. W. Nychka, and R. S. Stolarski, Statistical approaches to ozone trend detection, Appendix A, in *Global Ozone Research and Monitoring Project, Report of the International Ozone Trends Panel 1988, Vol. II*, 18, pp. 755-772, World Meteorol. Organ., Geneva, 1988.
- Bodeker, G. E., Trends in total column ozone over Australia and New Zealand and its influence on clear-sky surface erythema irradiance, *Radiat. Prot. Aust.*, 13, 39-49, 1993.
- Bureau of Meteorology, *Climate Activities in Australia*, Melbourne, Australia, 1995.
- Commission Internationale de l'Éclairage (CIE), *Sunscreen Testing (UV.B)*, Vienna, Austria, 1991.
- Dave, J. V., Meaning of successive iteration of the auxiliary equation of radiative transfer, *Astrophys. J.*, 140, 1292-1303, 1964.
- Drosowsky, W., An analysis of Australian seasonal rainfall anomalies: 1950-1987. I: spatial patterns, *Int. J. Climatol.*, 13, 1-30, 1993.
- Drosowsky, W., Variability of the Australian summer monsoon at Darwin: 1957-1992, *J. Clim.*, 9, 85-96, 1996.
- Drosowsky, W., and G. J. Holland, North Australian cloud lines, *Mon. Weather Rev.*, 115, 2645-2659, 1987.
- Drosowsky, W., G. J. Holland, and R. K. Smith, Structure and evolution of north Australian cloud lines, *Mon. Weather Rev.*, 117, 1181-1192, 1989.
- Duchêne, A. S., J. R. A. Lakey, and M. H. Repacholi (Eds.), Guidelines on limits of exposure to ultraviolet radiation of wavelengths between 180 nm and 400 nm (incoherent optical radiation), in *IRPA Guidelines on Protection Against Non-Ionizing Radiation*, chap. 3, pp. 42-52, Pergamon, Tarrytown, N.Y., 1991.
- Dütsch, H. U., Photochemistry of atmospheric ozone, *Adv. Geophys.*, 15, 219-222, 1971.
- Estupiñán, J. G., S. Raman, G. H. Crescenti, J. J. Streicher, and W. F. Barnard, Effect of clouds and haze on UV-B radiation, *J. Geophys. Res.*, 101, 16,807-16,816, 1996.
- Farman, J. C., B. G. Gardiner, and J. D. Shanklin, Large losses of ozone in Antarctica reveal seasonal ClO_x/NO_x interaction, *Nature*, 315, 207-210, 1985.
- Frederick, J. E., and D. Lubin, The budget of biologically active ultraviolet radiation in the earth-atmosphere system, *J. Geophys. Res.*, 93, 3825-3832, 1988.
- Frederick, J. E., and H. E. Snell, Tropospheric influence on solar ultraviolet radiation: The role of clouds, *J. Clim.*, 3, 373-381, 1990.
- Giles, G., and V. Thursfield, Trends in skin cancer in Australia, *Cancer Forum*, 20, 188-191, 1996.
- Green, A. E. S., J. Mo, and J. H. Miller, A study of solar erythema radiation doses, *Photochem. Photobiol.*, 20, 473-482, 1974a.
- Green, A. E. S., T. Sawada, and E. P. Shettle, The middle ultraviolet reaching the ground, *Photochem. Photobiol.*, 19, 251-269, 1974b.
- Herman, J., and E. Celarier (Eds.), *TOMS Version 7 UV-Erythema Exposure: 1978-1993 [CD-ROM]*, NASA Goddard Space Flight Center, Greenbelt, Md., 1996.
- Herman, J. R., and E. A. Celarier, Earth surface reflectivity climatology at 340-380 nm from TOMS data, *J. Geophys. Res.*, 102, 28,003-28,011, 1997.

- Herman, J. R., P. K. Bhartia, J. Ziemke, Z. Ahmad, and D. Larko, UV-B increases 1979-1992 from decreases in total ozone, *Geophys. Res. Lett.*, *23*, 2117-2120, 1996.
- Holton, J. R., P. H. Haynes, M. E. McIntyre, A. R. Douglass, R. B. Rood, and L. Pfister, Stratosphere-troposphere exchange, *Rev. Geophys.*, *33*, 403-439, 1995.
- International Light, IL 1700 Research Radiometer, *Data Sheet IL1700*, Newburyport, Mass., 1991.
- Iqbal, M., *An Introduction to Solar Radiation*, Academic, San Diego, Calif., 1983.
- Jones, P. A., Historical records of cloud cover and climate for Australia, *Aust. Meteorol. Mag.*, *39*, 181-189, 1991.
- Jones, P. A., and A. Henderson-Sellers, Historical records of cloudiness and sunshine in Australia, *J. Clim.*, *5*, 260-267, 1992.
- Kricker, A., and B. Armstrong, International trends in skin cancer, *Cancer Forum*, *20*, 192-195, 1996.
- Kuang, Z., Y. Jiang, and Y. Yung, Cloud optical thickness variations during 1983-1991: Solar cycle or ENSO?, *Geophys. Res. Lett.*, *25*, 1415-1417, 1998.
- Kylling, A., K. Stamnes, and S.-C. Tsay, A reliable and efficient two-stream algorithm for radiative transfer: Documentation of accuracy in realistic layered media, *J. Atmos. Chem.*, *21*, 115-150, 1995.
- Liu, S. C., and M. Trainer, Responses of the tropospheric ozone and odd radicals to column ozone change, *J. Atmos. Chem.*, *6*, 221-233, 1988.
- Lubin, D., and E. H. Jensen, Effects of clouds and stratospheric ozone depletion on ultraviolet radiation trends, *Nature*, *377*, 710-713, 1995.
- Madronich, S., Photodissociation in the atmosphere. 1. Actinic flux and the effects of close-up ground reflections and clouds, *J. Geophys. Res.*, *92*, 9740-9752, 1987.
- Madronich, S., Implications of recent total atmospheric ozone measurements for biologically active ultraviolet radiation reaching the surface, *Geophys. Res. Lett.*, *19*, 37-40, 1992.
- Madronich, S., The atmosphere and UV-B radiation at ground level, in *Environmental UV Photobiology*, edited by A. R. Young et al., chap. 1, pp. 1-39, Plenum, New York, 1993.
- McBride, J. L., and T. D. Keenan, Climatology of tropical cyclone genesis in the Australian region, *J. Climatol.*, *2*, 13-33, 1982.
- McBride, J. L., and N. Nicholls, Seasonal relationships between Australian rainfall and the southern oscillation, *Mon. Weather Rev.*, *111*, 1998-2004, 1983.
- McKenzie, R. L., Application of a simple model to calculate latitudinal and hemispheric differences in ultraviolet radiation, *Weather Clim.*, *11*, 3-14, 1991.
- McKenzie, R. L., W. A. Matthews, and P. V. Johnston, The relationship between erythral UV and ozone, derived from spectral irradiance measurements, *Geophys. Res. Lett.*, *18*, 2269-2272, 1991.
- McKinlay, A. F., and B. L. Diffey, A reference action spectrum for ultra-violet induced erythema in human skin, in *Human Exposure to Ultraviolet Radiation: Risks and Regulations*, edited by W. R. Passchier and B. F. M. Bosnjakovic, pp. 83-87, Elsevier, New York, 1987.
- McPeters, R., and E. Beach (Eds.), *TOMS Version 7 Reflectivity Data: 1978-1993 [CD-ROM]*, NASA Goddard Space Flight Center, Greenbelt, Md., 1996a.
- McPeters, R., and E. Beach (Eds.), *TOMS Version 7 O3 Gridded Data: 1978-1993 [CD-ROM]*, NASA Goddard Space Flight Center, Greenbelt, Md., 1996b.
- McPeters, R. D., and G. J. Labow, An assessment of the accuracy of 14.5 years of Nimbus 7 TOMS Version 7 ozone data by comparison with the Dobson network, *Geophys. Res. Lett.*, *23*, 3695-3698, 1996.
- McPeters, R. D., et al., Nimbus-7 Total Ozone Mapping Spectrometer (TOMS) Data Products User's Guide, *NASA Ref. Publ.*, 1384, 1996.
- Michelangeli, D. V., M. Allen, Y. L. Yung, D. C. Run-Sie Shia, and J. Eluszkiewicz, Enhancement of atmospheric radiation by an aerosol layer, *J. Geophys. Res.*, *97*, 865-874, 1992.
- Mims, F. M., and J. E. Frederick, Cumulus clouds and UV-B, *Nature*, *371*, 291, 1994.
- National Health and Medical Research Council, *Health Effects of Ozone Layer Depletion*, Australian Government Publishing Service, Canberra, Australia, 1989.
- Nicholls, N., B. Lavery, C. Frederiksen, W. Drosowsky, and S. Torok, Recent apparent changes in relationships between the El Niño - Southern Oscillation and Australian rainfall and temperature, *Geophys. Res. Lett.*, *23*, 3357-3360, 1996.
- Paltridge, G. W., and I. J. Barton, Erythral ultraviolet radiation distribution over Australia- The calculations, detailed results and input data, *Tech. Rep. 33*, CSIRO Div. of Atmos. Phys., Aspendale, Victoria, Australia, 1978.
- Randel, W. J., and J. B. Cobb, Coherent variations of monthly mean total ozone and lower stratospheric temperature, *J. Geophys. Res.*, *99*, 5433-5447, 1994.
- Robertson, D. F., Solar ultraviolet radiation in relation to human sunburn and skin cancer, Ph.D. thesis, University of Queensland, Brisbane, Australia, 1972.
- Rossow, W. B., and R. A. Schiffer, ISCCP cloud data products, *Bull. Am. Meteorol. Soc.*, *72*, 2-20, 1991.
- Roy, C., H. P. Gies, and S. Toomey, Monitoring UV-B at the Earth's surface, *Cancer Forum*, *20*, 173-179, 1996.
- Roy, C. R., and P. Gies, Ozone depletion and its calculated effect on solar UVB radiation levels for some Australian cities, in *Health Effect of Ozone Layer Depletion*, pp. 37-69, Nat. Health and Medical Res. Council, Canberra, Australia, 1989.
- Roy, C. R., H. P. Gies, and S. Toomey, The solar UV radiation environment: Measurement techniques and results, *J. Photochem. Photobiol. B*, *31*, 21-27, 1995.
- Ryer, A. D., *Light Measurement Handbook*, Int. Light, Newburyport, Mass., 1997.
- Schafer, J. S., V. K. Saxena, B. N. Wenny, W. Barnard, and J. J. D. Luisi, Observed influence of clouds on ultraviolet-B radiation, *Geophys. Res. Lett.*, *23*, 2625-2628, 1996.
- Seckmeyer, G., R. Erb, and A. Abold, Transmittance of a cloud is wavelength-dependent in the UV-range, *Geophys. Res. Lett.*, *23*, 2753-2755, 1996.
- Shettle, E. P., and J. A. Weinman, The transfer of solar irradiance through inhomogeneous turbid atmospheres evaluated by Eddington's approximation, *J. Atmos. Sci.*, *27*, 1048-1055, 1970.
- Shiotani, M., Annual, quasi-biennial, and El Niño-Southern Oscillation (ENSO) time-scale variations in equatorial total ozone, *J. Geophys. Res.*, *97*, 7625-7633, 1992.
- Simmonds, I., and P. Hope, Persistence characteristics of Australian rainfall anomalies, *Int. J. of Climatol.*, *17*, 597-613, 1997.
- Stolarski, R. S., P. Bloomfield, R. D. McPeters, and J. R. Herman, Total ozone trends deduced from Nimbus 7 TOMS data, *Geophys. Res. Lett.*, *18*, 1015-1018, 1991.
- Supiah, R., The Australian summer monsoon: A review, *Prog. in Phys. Geogr.*, *16*, 283-318, 1992.
- Svensmark, H., and E. Friis-Christensen, Variation of cosmic ray flux and global cloud coverage-A missing link in solar-climate relationships, *J. Atmos. Sol. Terr. Phys.*, *59*, 1225-1232, 1997.
- Tinsley, B. A., Correlations of atmospheric dynamics with solar wind-induced changes of air-earth current density

- into cloud tops, *J. Geophys. Res.*, *101*, 29,701–29,714, 1996.
- Tung, K. K., and H. Yang, Global QBO in circulation and ozone, I, reexamination of observational evidence, *J. Atmos. Sci.*, *51*, 2699–2707, 1994a.
- Tung, K. K., and H. Yang, Global QBO in circulation and ozone, II, a simple mechanistic model, *J. Atmos. Sci.*, *51*, 2708–2721, 1994b.
- Warren, S. G., C. J. Hahn, J. London, R. M. Chervin, and R. L. Jehne, Global distribution of total cloud cover amounts over land, technical notes, NCAR/TN-273+STR, Nat. Cent. of Atmos. Res., Boulder, Colo., 1986.
- Weatherhead, E. C., G. C. Tiao, G. C. Reinsel, J. E. Frederick, J. J. DeLuisi, D. Choi, and W.-K. Tam, Analysis of long-term behavior of ultraviolet radiation measured by Robertson-Berger meters at 14 sites in the United States, *J. Geophys. Res.*, *102*, 8737–8754, 1997.
- Williams, G., and A. Green, A cumulative-exposure model for predicting the increase in non-melanoma skin cancer associated with ozone depletion, *Cancer Forum*, *20*, 195–198, 1996.
- Yang, H., and K. K. Tung, On the phase propagation of extratropical ozone quasi-biennial oscillation in observational data, *J. Geophys. Res.*, *100*, 9091–9100, 1995.
-
- P. Gies and C. Roy, Ultraviolet Radiation Section, Non Ionizing Radiation Branch, Australian Radiation Protection and Nuclear Safety Agency, Lower Plenty Road, Yallambie, VIC 3085, Australia. (e-mail: peter.gies@health.gov.au; colin.roy@health.gov.au)
- W. J. Randel, National Center of Atmospheric Research, Atmospheric Chemistry Division, PO Box 3000, Boulder, CO 80307-3000. (e-mail: randel@acd.ucar.edu)
- P. M. Udelhofen, Institute for Terrestrial and Planetary Atmospheres, State University of New York at Stony Brook, MSRC/Endeavour Hall, Stony Brook, NY 11794-5000. (e-mail: pudelhofen@notes.cc.sunysb.edu)

(Received October 13, 1998; revised February 19, 1999; accepted April 19, 1999.)